We are IntechOpen,
the world's leading publisher of
Open Access books
Built by scientists, for scientists

4,800
Open access books available

122,000
International authors and editors

135M
Downloads

Our authors are among the

154
Countries delivered to

TOP 1%
most cited scientists

12.2%
Contributors from top 500 universities

CLARIVATE ANALYTICS
BOOK CITATION INDEX
INDEXED

WEB OF SCIENCE™

Selection of our books indexed in the Book Citation Index
in Web of Science™ Core Collection (BKCI)

Interested in publishing with us?
Contact book.department@intechopen.com

Numbers displayed above are based on latest data collected.
For more information visit www.intechopen.com

Self-healing of Structural Composites Containing Dendrimers as Healing Agent

Vassilis Kostopoulos and Athanasios Kotrotsos

Additional information is available at the end of the chapter

Abstract

Dendrimers exhibit healing functionalities on polymer level. In the present chapter, the effect of hydrogen-bonded supramolecular polymers (SP) into high performance aerospace carbon fiber reinforced plastics (CFRPs) is assessed. More precisely, the interlaminar fracture toughness of unidirectional (UD) SP-modified composites (containing SP interleaves) and their healing capability were measured under mode I and mode II fracture loading conditions. During testing, these modified samples exhibited extended bridging between the interlaminar crack flanks, which considerably enhanced their interlaminar fracture toughness. Furthermore, SP pre-impregnated fiber layers (prepregs) were fabricated to facilitate the introduction of the self-healing agent (SHA) into the composite laminated structure. SP prepregs were used to modify quasi-isotropic CFRPs in a symmetric fashion, and the damage tolerance of the modified composites was investigated. To that direction, the SP-modified laminates were tested under low velocity impact (LVI) conditions, and compression after impact (CAI) tests were conducted prior and after the activation of the healing. Finally, examination of the morphology of fracture surface led to qualitative conclusions regarding the involved failure and healing mechanisms.

Keywords: composites, self-healing, hydrogen bonds, supramolecular polymers, fracture mechanics, damage tolerance

1. Introduction

1.1. Background

During the last decades, the use of composites in aeronautics, wind energy, automotive, and other mechanical engineering applications has been significantly increased. The need for new materials with enhanced mechanical properties, low density and corrosion resistance combined
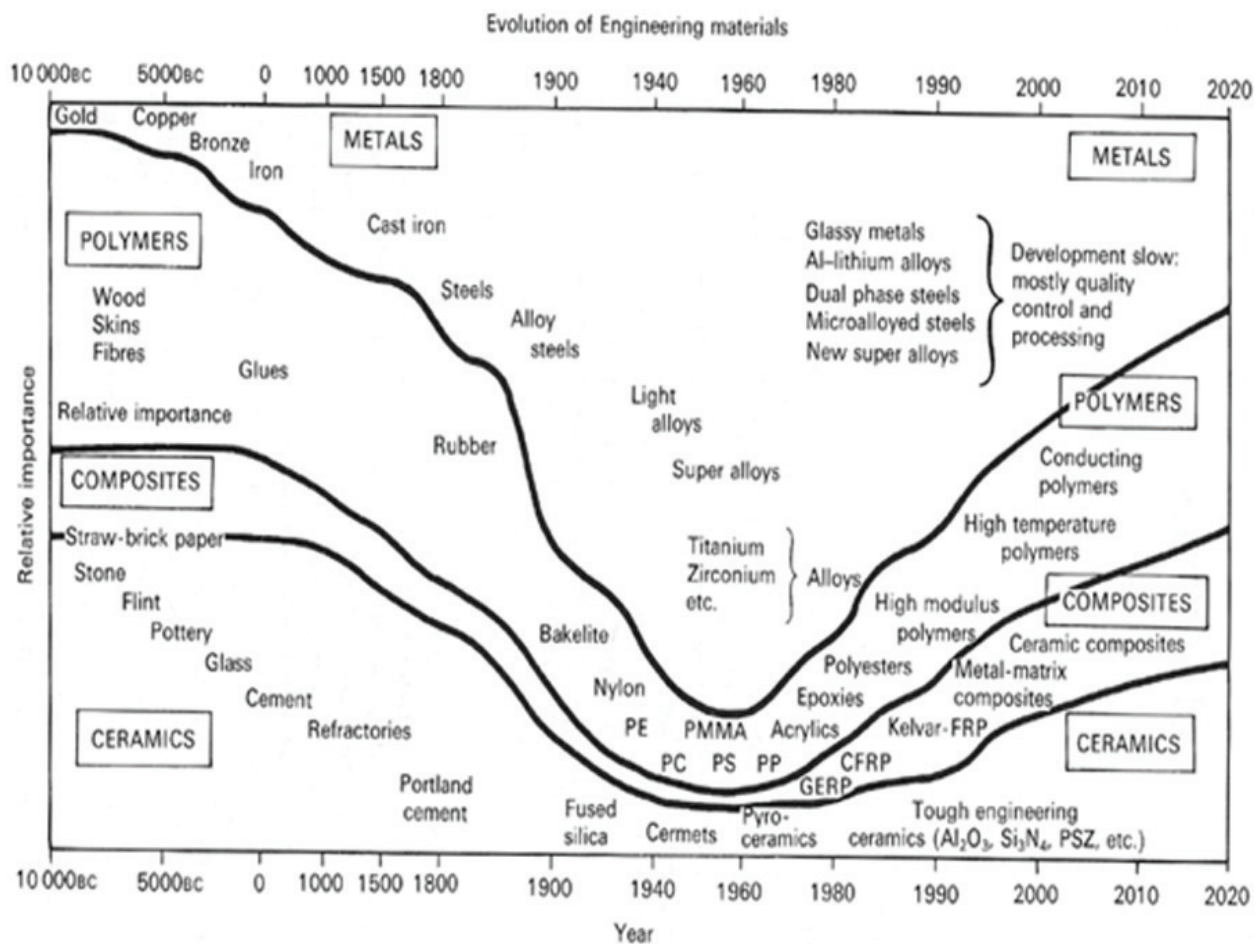
Figure 1. Schematic representation of the importance of four classes of materials (ceramics, composites, polymers, and metals) in mechanical and civil engineering as function of time [1].

with the necessity for greener operation of structures, was the main driver for intensive research and application of polymer-matrix-fiber-reinforced composites in many fields as structural materials. **Figure 1** shows the evolution in use of materials versus time. In this picture, the rapid increase in the use of polymers and composite materials, during the last decades is evident [1].

In addition, the use of composites and, especially, carbon/epoxy composites in aerospace applications has been considerably increased since 1960. Characteristic examples are Boeing 787 Dreamliner and Airbus 350-XWB in which their structural mass is made by 50 and 55% of composites, respectively. As it is expected, the extensive use of composites results to more fuel efficient and environmental friendly aircrafts. However, a primary limitation of composites is their poor interlaminar strength and fracture toughness that make them prone to delaminations [2, 3]. In [4], possible damage modes into a polymer composite are described in detail. Delamination is the result of out of plane LVI of a composite structure. Joining of the microcracks, developed into the polymer matrix under service loads, is another option for delaminations. It is obvious that delaminations can lead to significant suppression of the load-bearing capacity of the composite components and structures.

During the last decades, significant research effort has been invested to the improvement of interlaminar fracture performance of structural composites and especially of CFRPs. A variety

of methodologies have been proposed in the literature to prevent composites from delaminations. These include chemical modification of epoxy matrix systems (either by modifying the resin or the hardener), interleaving, hybridization, stitching, short-fibers, z-pinning, optimization of staking sequence, reactive rubbers and edge-cap reinforcement [5–14]. However, although the interlaminar fracture properties have been enhanced, delamination remains the main damage mode in the case of FRPs. Furthermore, conventional repair techniques [15, 16] of composites are time consuming, require extensive labor cost, and the repair defects face certain restrictions. These repair techniques involve patch repair (e.g., bonded external patch, bonded flush patch) or non-patch repair (e.g., resin injection, potting or filling and surface coating) [15, 16]. In the case of repair of primary structural components, the certification authorities required additional mechanical joining. **Figure 2(a)** illustrates a representative example of patch repair method in which the damage material is carefully removed by using a high-speed grinder [15]. After material removal, new composite plies are utilized to fill the created cavity. On the other hand, **Figure 2(b)** shows non-patch repair which includes resin injection through an access hole into the damage area. This method eliminates the removal of undamaged plies and results in higher recovery of the strength [16].

Thus, utilization of composites in human safety critical components has always to be accompanied with non-destructive testing techniques (NDTs) as damage monitoring tool. These techniques involve ultrasonics, surface waves, Acoustic emission, infrared thermography, and X-ray radiography [16]. It is also of note that conventional damage detection equipment is, in some cases, not able to detect tiny defects deep inside the material. However, these defects could rapidly propagate between two periodical inspections and lead the composite part to significant deterioration. This challenging situation acted as an inspiration for seeking of new repair methods; cheaper and applicable at the early stages of damage evolution. With an aim to address some principal weak points of conventional repair techniques, an emerging approach called "self-healing materials" [17, 18] has been proposed but not yet been applied to commercial composites. This smart technology aims to in-situ and autonomously repair damage and thus to lead to extension of the effective life-span of composite structures. Self-healing of
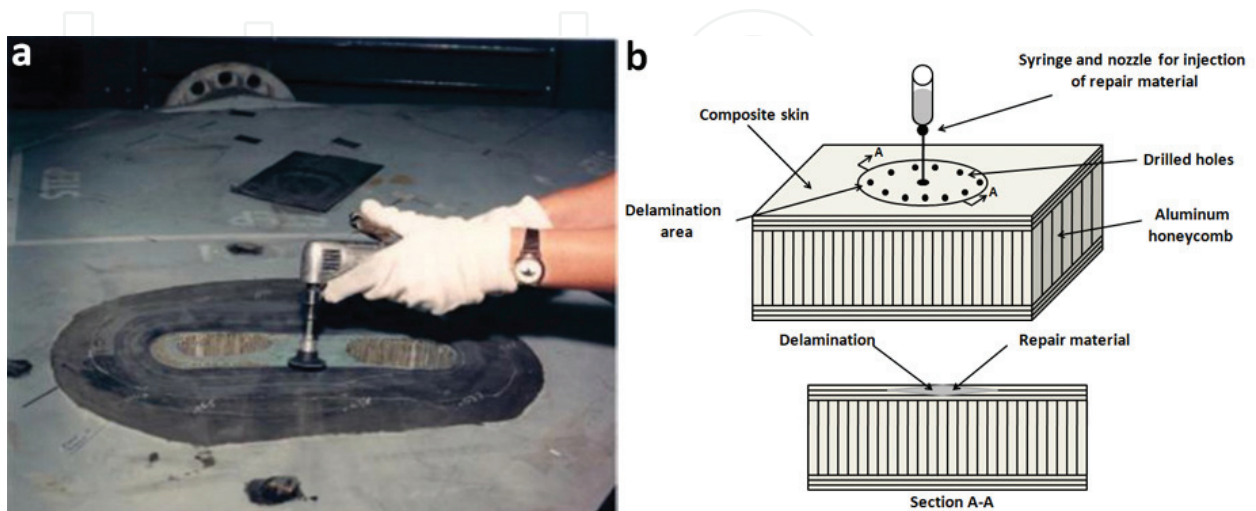

Figure 2. (a) Scarf cavity formation prior to patch repair [15]. (b) Depiction of the resin injection process into honeycomb panel skin's composite.

composites promises to mitigate the importance for detecting damage and to reduce the frequency of scheduled inspections.

Self-healing mechanisms incorporated into existing materials is an emerging alternative to conventional repair methods to remove cracks and restore performance. It is also considered as an intense research field over the last decades. A self-healing material [19] is a class of biomimetic materials that can autonomously repair damage and regain its initial properties after damage. Self-healing technologies could extend the service life and reliability of epoxy resins and their composites. Based on published research work, a typical way to classify self-healing systems is as: (a) autonomous (extrinsic) [20, 21] (capsule-based systems [20] or vascular-based systems [21]), where a container is prefilled with a liquid self-healing agent (SHA). (b) Non-autonomous [22, 23], where self-healing is created either by using a modifier with inherently reversible behavior [22] or by incorporating functional groups directly into a thermoset structure that can form reversible bonds (intrinsic [23]). While for non-autonomous self-healing, an external stimulus (heating) is required, autonomous self-healing operates at service temperature (not external stimulus is required).

A new technology that could be beneficial for self-healing in composites has been built on dendrimers (SP) [24]. Especially those based on reversible hydrogen bonding arrays show great promise as self-healing materials [25–27], since these materials can typically withstand multiple healing cycles without substantial loss of performance, because of the highly directional and fully reversible non-covalent interactions present into the polymer matrix. During the last decades, many types of dendrimers have been reported and are classified according to the type of the non-covalent bond involved. Dendrimers are classified into the following categories: SP based on hydrogen bonds [25–27], SP based on π-π stacking interaction [28], SP based on metal ligand interaction [29], and SP based on ionomer [30]. In the present chapter, the ureiodypyrimidone hydrogen bonding unit (UPy) as developed by Meijer and coworkers [27] has been employed because of its strong self-association, its synthetic accessibility, and the highly dynamic nature of low T_g-polymers comprising the UPy [31]. Most interestingly, UPy-polymers have recently been shown to give unprecedented toughening in polybutadiene-based interpenetrating networks [32].

In the present chapter, interleaves comprising self-healing materials based on hydrogen-bonded SP were successfully incorporated into high performance UD carbon/epoxy composites. The interlaminar fracture toughness of these modified composites and their healing capabilities were measured under mode I and II fracture loading conditions (Sections 3 and 4, respectively). During testing, these modified samples exhibited extended bridging phenomena, which considerably enhanced the interlaminar fracture toughness of the composites. Potential knock-down effect by the incorporation of the SP interleaf was quantified through three-point bending tests (3PB). Furthermore, SP carbon fiber prepregs were fabricated to simplify the incorporation process of SHA into the composite laminates. SP prepregs were further utilized to modify quasi-isotropic CFRPs. Potential knock-down effects and the induced healing capability of these modified composites were investigated under LVI and CAI tests. Finally, examination of the morphology of fracture surface led to qualitative conclusions regarding the involved failure and healing mechanisms.

2. Experimental

2.1. Materials and methods

2.1.1. Materials

The SP-modified composite laminates, which are used in the present chapter, were fabricated by UD carbon fiber/epoxy resin prepreg CE-1007 150-38. The prepreg tape material supplied by SGL Group, Germany having tensile strength of 2.4 GPa and axial Young modulus of 140 GPa. The SP was developed and supplied by Suprapolix, the Netherlands. The supplied material (batch identification code: SPSH01) is based on a low T_g ($-66°C$) polymer modified with UPy moieties.

2.1.2. Preparation of the SP interleaves and SP prepreg plies

The preparation process of the SP interleaves and prepregs are illustrated in **Figure 3**. The as-received polymer piece (**Figure 3(ai)**) was converted into a thin film by a two-step heating/pressuring treatment (**Figure 3(aii)**) using a hot press machine. On the other hand, the preparation process of the SP prepreg is illustrated in **Figure 3(b)**. Raw SP pieces (**Figure 3(bi)**) were placed on the top and bottom surfaces of dry UD carbon fabric. Then, the system was placed in between two Polytetrafluoroethylene (PTFE) films and converted into SP prepreg by a two-step heating/
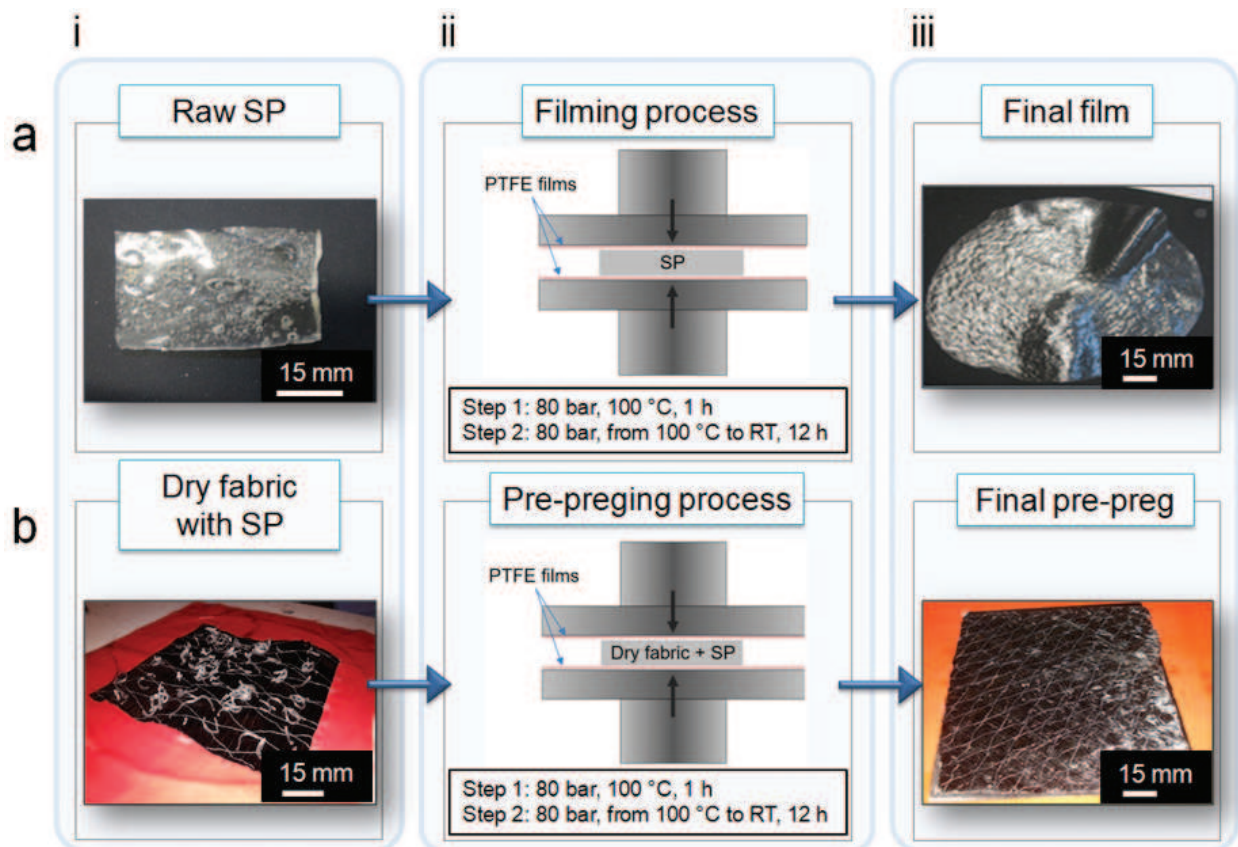

Figure 3. (a) Filming process of the SP and (b) preparation process of the SP-modified prepreg plies.

pressing treatment (**Figure 3(bii)**) using a hot press machine. Firstly, both systems were pressed under 80 bars at 100°C for 1 h. Then, heating was stopped and both the SP film and prepreg were left under 80 bars applied pressure overnight to cool down and reach their final form (**Figure 3 (aiii, biii)**). The thickness of the film and prepreg was measured to be approximately 120 μm and 180 μm, respectively, with no significant thickness variations, using a digital caliper.

2.1.3. Mode I interlaminar fracture toughness testing

Quasi-static interlaminar fracture toughness tests described in Section 3 were performed at a 25 kN Instron Universal testing machine (Instron, High Wycombe, UK) at RT conditions. The mode I interlaminar fracture toughness was measured using the double cantilever beam (DCB) method according to the AITM 1.0005 standard issued by Airbus. DCB specimen dimensions and experimental setup are both illustrated in **Figure 5**. The 25-mm-long PTFE starter film that was placed at the central plane, at one edge of the samples to facilitate crack initiation is also shown. Two aluminum tabs were glued on the outer surfaces of the pre-cracked end of the specimens, for the application of the opening load. The specimens were loaded in tension at a cross-head velocity of 10 mm/min until the crack was propagated from starting point considered as zero to 75 mm. Five samples were tested each time for the calculation of G_{IC}. The mode I interlaminar fracture energy of the CFRPs was calculated using Eq. (1),

$$G_{IC} = \frac{A}{aw} \cdot 10^3 \left(\frac{kJ}{m^2} \right)$$

(1)

where, A is the required energy to achieve the total propagated crack length, a is the propagated crack length (final crack length minus initial crack length, a = 75 mm), and w is the specimen's width.

2.1.4. Mode II interlaminar fracture toughness testing

The mode II interlaminar fracture toughness tests described in Section 4 were measured using the three-point end-notched flexure (ENF) method according to the AITM 1.0006 standard issued by Airbus. Firstly, the DCB specimens were loaded under mode I in alignment with the AITM 1.0005 to create a natural sharp pre-crack. Then, the delaminated specimens were cut into ENF specimens as shown in **Figure 15**, according to AITM 1.0006. ENF specimen dimensions and experimental setup are both illustrated in **Figure 15**. The pre-cracked ENF specimens were subjected to flexural loading that generated a shear crack driving force at the crack tip region. The cross-head velocity was fixed at 1 mm/min. Five samples were tested for each fracture toughness assessment. The G_{IIC} was determined using Eq. (2),

$$G_{IIC} = \frac{9Pa^2d}{2w(\frac{1}{4}L^3 + 3\alpha^3)} \left(\frac{kJ}{m^2} \right)$$

(2)

where, d is the cross-head displacement at crack delamination onset, P is the critical load to start the crack, α is the initial crack length (from the support point to the end of the crack, α = 35 mm), w is the width of the specimen, and L is the span length (L = 100 mm). For accurate calculation of the G_{IIC}, the simple methodology described was applied.

2.1.5. Low velocity impact and post-impact testing

The core objective of the current characterization program, which is described in Section 5, is the determination of the low velocity impact resistance and the compression strength after impact of the proposed modified CFRP systems, since these characteristics dominate the damage tolerance of the composite material system. The LVI and CAI tests were performed at RT conditions according to AITM1-0010: 2015 standard of Airbus. A guided drop weight tester was utilized for this purpose. A drop tower equipped with a 16-mm diameter hemispherical aluminum impactor weighing 2.5 kg was employed. The selected impact energy was 25 J and was delivered by adjusting the initial height of the impactor. The impactor was manually left to fall from the pre-determined height and was arrested automatically after rebounding to avoid a second strike. The residual compressive strength of the damaged CFRP plates before and after the healing process was measured through CAI tests. For this purpose, an anti-buckling jig was employed to support the specimen edges and to inhibit Euler buckling. All tests were conducted at an Instron (250 kN) hydraulic machine. The specimens were loaded under displacement control of cross-head velocity of 0.5 mm/min.

2.1.6. Composites quality issues

C-scan inspection was performed on all the manufactured plates. A Physical Acoustics Corporation (PAC) UT C-Scan system was used with a 5 MHz transducer. C-scan images of plates intended for mode I, mode II, and LVI tests confirmed good qualities and showed absence of porosity and delaminations due to the manufacturing process.

2.1.7. Healing procedure and healing efficiency calculations

After first crack propagation under mode I or mode II or delamination damage due to LVI described below (Sections 3–5, respectively), the specimens were subjected to a simple healing cycle of heating under controlled through-the-thickness compression. The cycle comprised a 15 min dwell at $100°C$ under loading of 1 kN for mode I & II samples, while of 5 kN through the thickness compressive force was used for LVI samples, using a heat press machine. The applied temperature was chosen to be $23°C$ higher than the T_m value (approximately $77°C$) of the SP material, for 15 min, in order to be sure that the SP will flow between the crack flanks and to achieve the healing effect. The healing temperatures were chosen based on previous in-house differential scanning calorimetry (DSC) measurements. The compressive loading value was chosen as the minimum necessary to ensure that the adjacent crack flanks were kept in close proximity during healing activation. The loading values were chosen as the minimum necessary to ensure that the adjacent crack flanks were kept in intimate contact during the healing procedure. Then, the samples were left to cool down at room temperature (RT). After the healing cycle, the samples were tested again using the same configurations. The calculations of the healing efficiency (HE) of every system were based on Eq. (3) for mode I and II tests and on Eq. (4) for LVI tests:

$$HE = \frac{M_{healed}}{M_{modified}} \cdot 100 \ (\%) \tag{3}$$

$$HE = \frac{S_{healed}}{S_{damaged}} \cdot 100 \ (\%) \tag{4}$$

where M or S (i.e., damage area) is the property under examination. M_{healed} and $M_{modified}$ are the values of the property after healing and before healing, respectively. S_{healed} and $S_{damaged}$ are the values of the property after healing and after LVI testing, respectively.

3. Mode I interlaminar fracture toughening and healing of carbon fiber/epoxy composites by hydrogen-bonded supramolecular polymer interlayers as SHA

3.1. Composites manufacturing

Two UD laminated plates made of 22 layers were manufactured for the needs of the current study; the reference plate and the modified one containing the SP interleafs at the mid-plane, both appropriate for mode I interlaminar fracture tests. **Figure 4** shows schematically the plate configuration. The dimensions of the plates were 300 mm × 150 mm × 3 mm. During the manufacturing process, two 13-μm-thick sheets of PTFE film were placed in the mid-thickness plane of both laminates as shown in **Figure 4**, to act as initial pre-crack according to the request of the interlaminar fracture test. In the case of the modified laminate, SP strips were carefully placed at the mid-plane as shown in **Figure 4(b, c)**.

Following the lay-up, the laminates were vacuum bagged and cured in autoclave for 2 h at 130°C under 6 bars applied pressure, according to the prepreg manufacturer guidelines. The fiber volume fraction of all manufactured plates was calculated to be close to 60%. Moreover, the incorporation of the SP film in the mid-plane of the modified laminate did not appear to
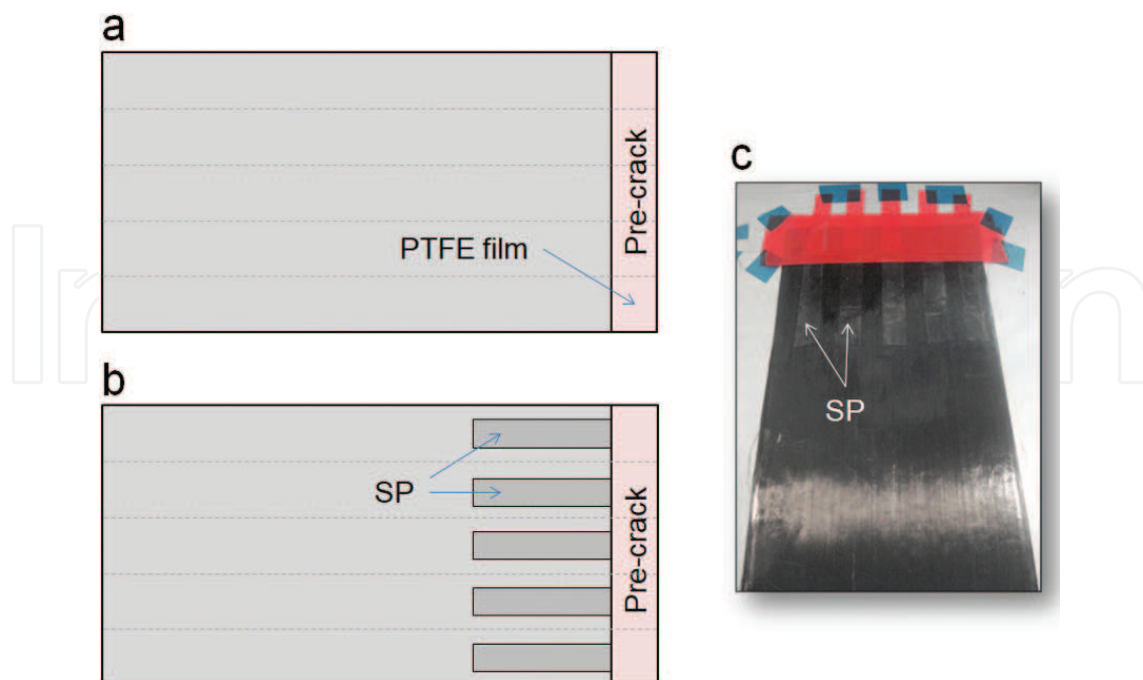

Figure 4. Schematic representation of (a) the reference plate and (b) the modified plate. (c) Photograph of the mid-plane placement of SP film, together with the PTFE initial crack formation.
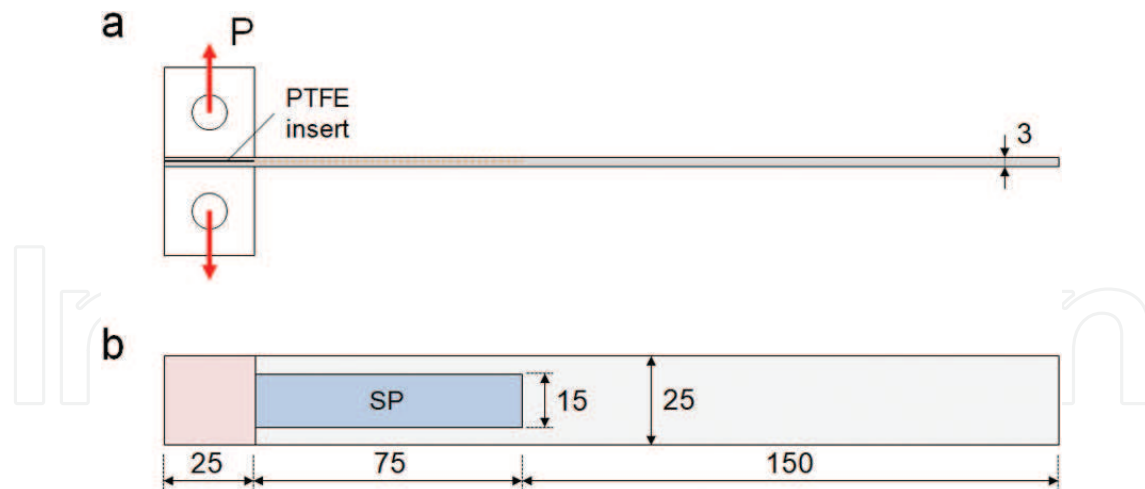
Figure 5. Schematic depiction of the modified DCB test specimen configuration. (a) Side view. (b) Top view. Dimensions in mm.

have a significant effect on the densities and the thicknesses of the samples. Five mode I samples were cut from both the reference and the modified plate. Two aluminum tabs were glued on the DCB specimen outer surfaces (**Figure 5**) using a two-component epoxy adhesive in order to apply the peel/opening forces.

3.2. Results and discussion

The study is deployed in two levels. The first level covers the assessment of the performance change due to the introduction of the SHA in the reference CFRP system. It is possible that the approach to introduce the healing functionality may jeopardize the load-bearing capacity of the composite. This change in performance is commonly referred to as the knock-down effect. The second level of this study deals with the healing functionality of the composite system and its performance. Essentially, once the SHA has been incorporated, the system is expected to have a healing functionality; meaning the capability to heal damage in the form of cracks (externally activated). The extent to which this functionality delivers its purposes is assessed in the second level of this work. Details on the procedure are given in the next paragraph.

3.2.1. Mode I fracture toughness: reference versus modified CFRP

The introduction of the SHA in the CFRP laminate is expected to have an impact on the material performance. In this paragraph, the impact of SHA on the mode I interlaminar fracture toughness is assessed according to specifications described in Section 2.1.3. To this purpose, load-displacement measurements were performed on the pre-cracked samples under mode I peel loading. The concluded load-displacement curves for the reference as well as for the SHA-modified samples are depicted in **Figure 6(a)**. For both composite DCB specimens, the applied load initially increased linearly prior the interlaminar pre-crack start to propagate, followed by a deviation from linearity and ended with a load drop as the crack starts to propagate. It is important to notice that the modified laminate that comprises the SP film as
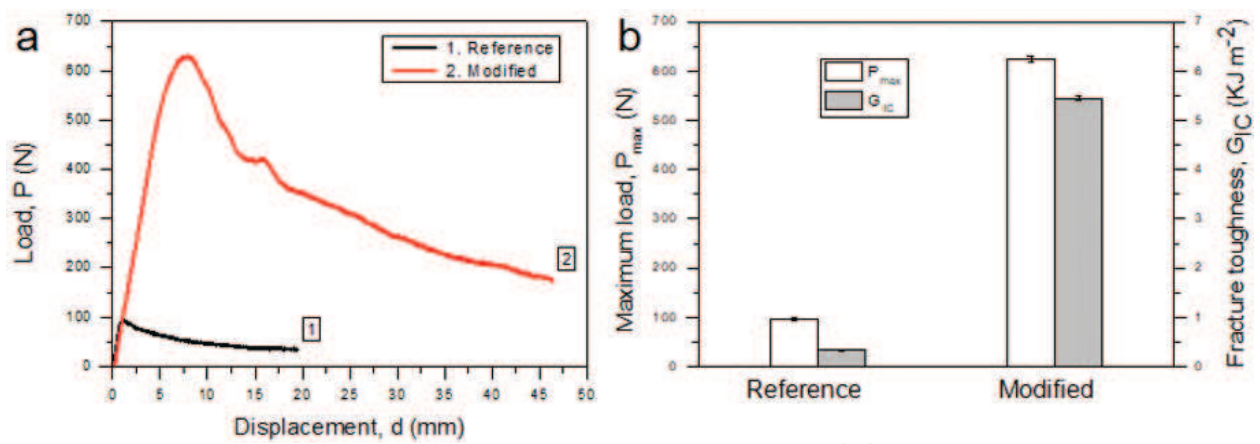
Figure 6. (a) Representative load (P) versus crack opening displacement (d) curves during the mode I interlaminar fracture toughness test of the reference and the modified CFRPs. (b) Comparison between the reference and the modified CFRP in terms of the P_{max} and the G_{IC} values, respectively.

interleaf in its mid-plane, displays a significantly higher P_{max} and calculated G_{IC}, when compared to the reference laminate without SP interleave (**Figure 6(b)**).

Figure 7 illustrates the bridging that occurs during crack propagation, resulting from the presence of the SP film in between the upper and lower crack surfaces of the sample. The crack appeared to propagate through the SP interleaf rather than along the SP/thermoset interface. Clearly, the presence of the SP interleaf reduces the crack opening displacement at a given applied load, due to the developed bridging within the crack flanks, and thus results in a lowering of the stress at the crack tip, and consequently in an increased mode I interlaminar
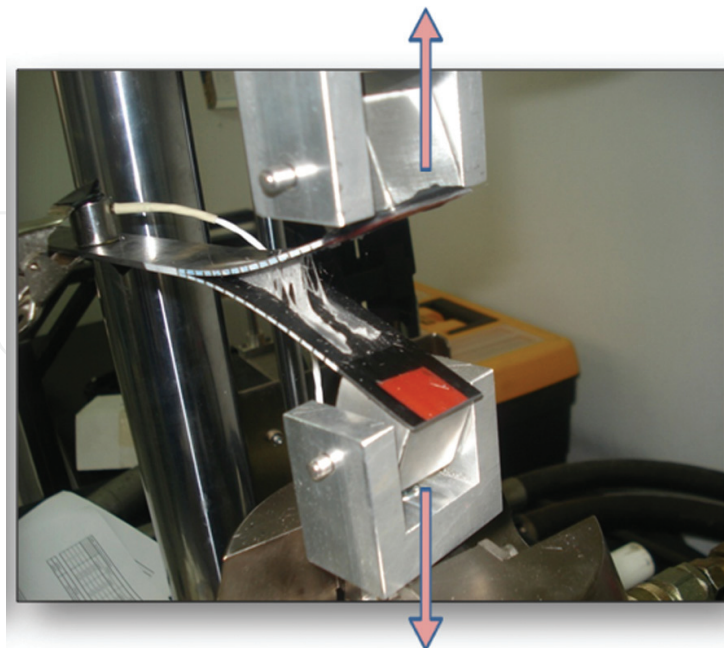

Figure 7. Illustration of the extended bridging phenomenon of the SP interleaf between the upper and the lower adjacent surfaces during mode I tests.

fracture toughness. Furthermore, the SP material displayed a high peel resistance. The results clearly show that the presence of the SP interleave in the plate resulted not only in a considerable increase of P_{max} (545%) but even more into a calculated G_{IC} that was increased with more than one order of magnitude (1550%).

Typical crack opening resistance curves (R-curves) under mode I loading conditions for the reference and the SP-modified composites are depicted in **Figure 8**. The G_{IC} value in composite laminates is of great importance, since it controls the initiation and the propagation of the delamination damage. As it is shown in **Figure 8**, the reinforcing effect of the SP film is apparent. The presence of the SP interleaf promotes the development of a bridging traction zone at the interlaminar region, which suppresses the crack tip opening stresses and as a result increases the resistance of the composite to both the initiation and the propagation of the delamination damage. The R-curve for the reference composite shows the plateau value already after reaching a crack length of 30 mm, resulting in a very limited damage process zone (lower than 5 mm). On the other hand, the R-curve for the SP-modified interleaf composite shows the plateau value only after reaching a crack length of 45 mm. This results in an extended damage process zone followed by a self-similar crack propagation pattern showing the typical delamination evolution mechanism up to a crack growth length of 80 mm and eventually resulting in a significant reduction of G_{IC} value at longer crack lengths.

The significant toughness increase observed for the modified interleaf is attributed to the enhanced SP material interface with the epoxy matrix, which is extremely strong thereby forming strong bonding between the SP polymer and the epoxy resulting in a transfer of the propagation of delamination to the SP material. This enhanced interface is visible in **Figure 9(b)**,
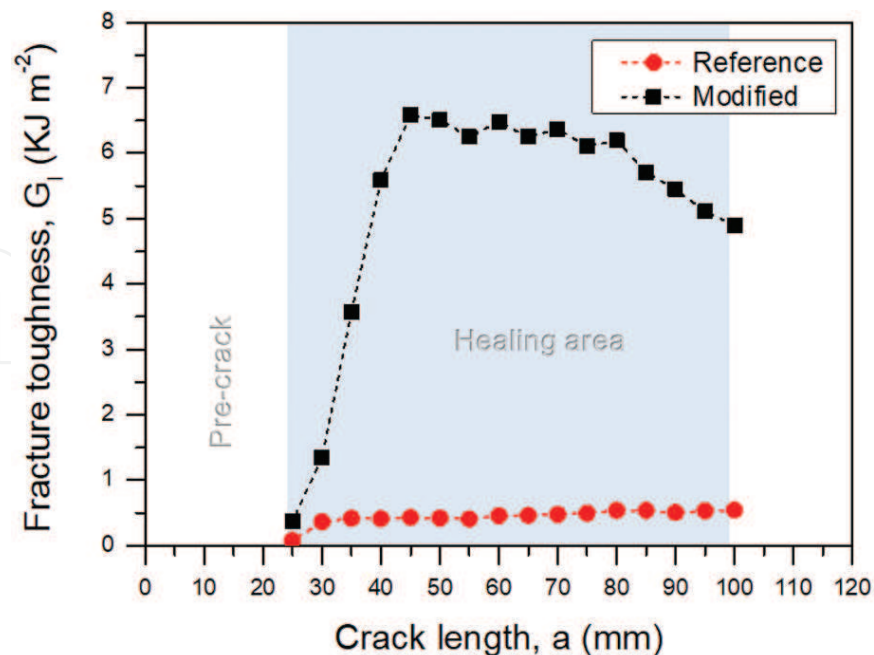

Figure 8. Representative R-curves of the reference and the modified CFRPs, showing the relation between G_I and crack length (a).
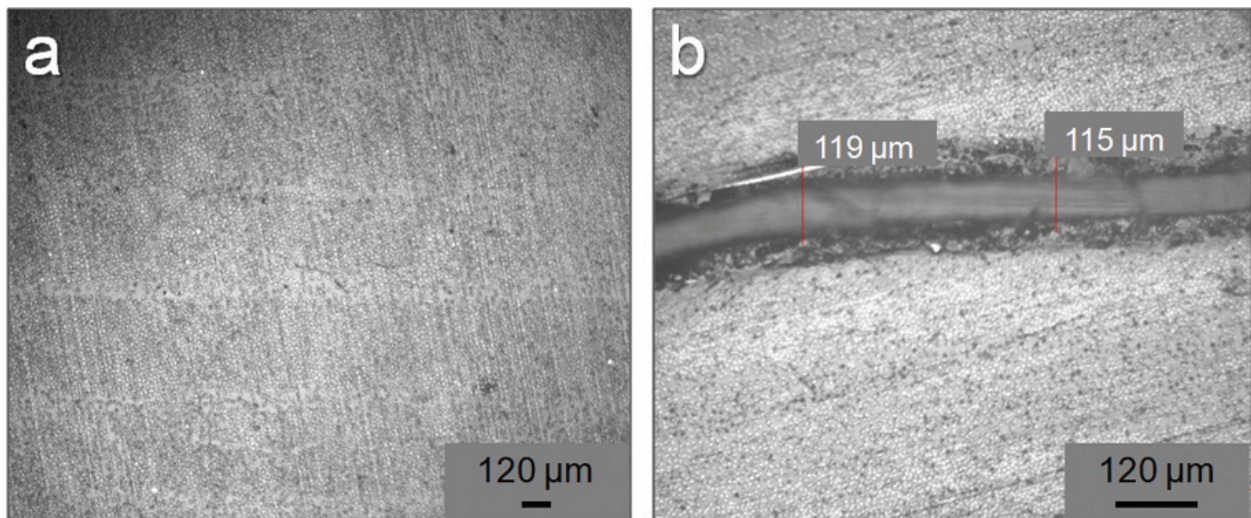
Figure 9. Cross section of the (a) reference and (b) SP interleaved-modified composite.

which shows infiltration by the SP material into the epoxy matrix as evidenced by the darkened region of the matrix next to SP interleaf.

In addition, there is also a clear difference between the failure types of the matrix. The reference material clearly shows brittle matrix failure with intact carbon fibers as observed with optical microscopy (**Figure 10(a)**). In contrast, the matrix of the SP-modified interleaf composite shows ductile failure, since both fracture surfaces are covered with the SP interleaf comprising partially pulled-out carbon fibers emanating from the edges of the SP film that the epoxy system exists (**Figure 10(b, c)**). This behavior reveals the strong bonding of the SP interleaf with both the matrix and the carbon fibers due to the infiltration. This strong bonding is foreseen to inhibit crack propagation because of the extra energy required for interfacial failure. In this turn, interfacial failure leads to frictional sliding and/or plastic deformation at the interface and finally to the propagation of delamination through the SP material as well as carbon fibers breakage or pull-out and crack bridging. Another characteristic of the SP was the formation of agglomerates on fractured surfaces locally, after the fracture of the SP interleaf (**Figure 10(d)**), probably originating from yielded SP bridges at the delamination interfaces.

3.2.2. Assessment of healing functionality of composites

The ability of these SP interleafs for self-healing of the cracked CFRP composites was investigated by subjecting the samples after the interlaminar crack propagation under mode I loading to a healing cycle of heating and compression of the laminates at 100°C for 15 min under a compressive load of 1 kN, as described in Section 2.1.7. Indeed, when the fractured samples had been removed from the loading frame after the mode I interlaminar fracture tests, and had been subjected to this healing cycle, a large recovery of the interlaminar fracture performance was observed. As can be seen in the resulting load-displacement curves for the SP-modified composites before and after the healing (**Figure 11(a)**), recovery of around 60% of P_{max} and G_{IC} values after the first healing cycle were monitored. In subsequent healing cycles on the same samples, a
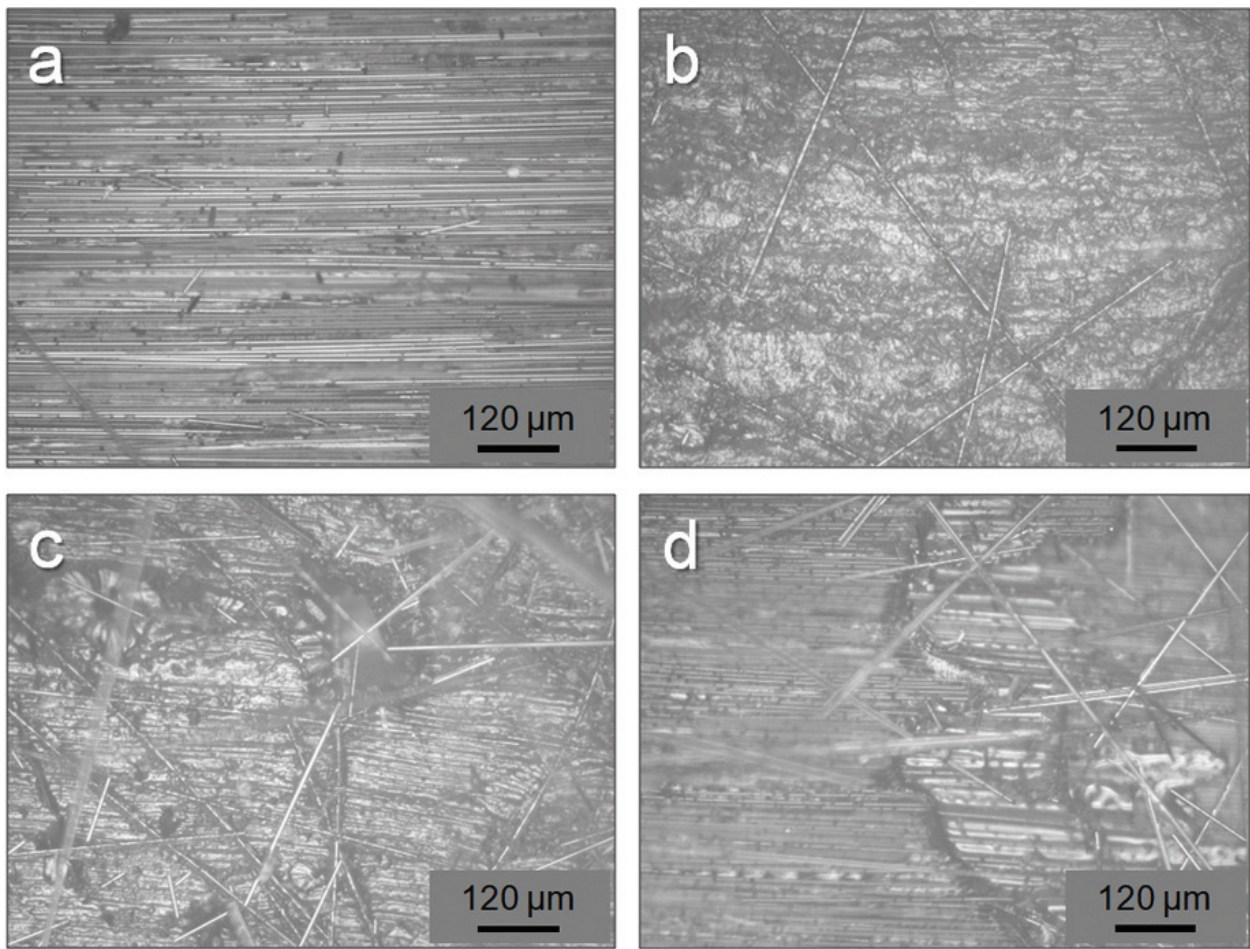
Figure 10. Fracture surfaces of the CFRPs. (a) Reference. (b) Bottom fracture plane of the SP interleaf-modified CFRP. (c) Top fracture plane of the SP interleaf-modified CFRP. (d) Illustration of the agglomerates on the top fracture plane of the modified CFRP. In the left side (of image (d)), the epoxy area is distinguished, while in the right side, the infiltrated area is distinguished by the SP material (photograph taken from the edge of the SP interleaf).
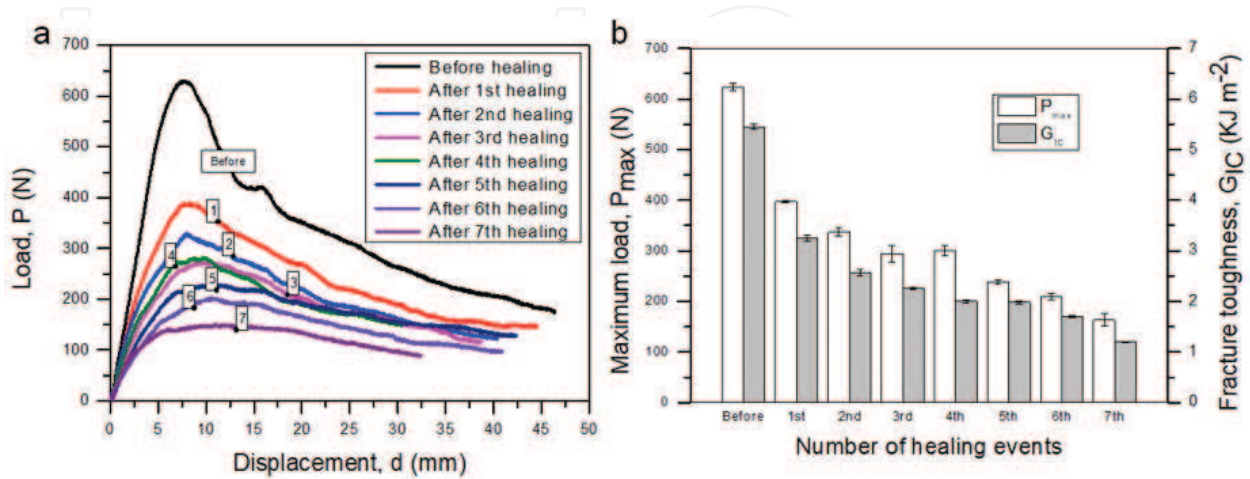

Figure 11. (a) Representative load (P) versus crack opening displacement (d) curves before and after the healing cycles during the mode I experiments. (b) Bar diagrams for the P_{max} and G_{IC} values, before and after the healing cycles in mode I experiments.

drop in HE was observed after each cycle until the recovery of P_{max} and G_{IC} values, after the seventh healing cycle, dropped at the level of 26 and 22%, respectively, when compared to the pristine samples (**Figure 11(b)**). Although, the bridging of crack flanks was still there during mode I interlaminar loading for the healed samples, its efficiency appeared to decrease with increasing number of healing cycles.

The ability of the healing interleaf to heal the cracks and to recover the fracture properties depends highly on the ability of the SP material's chains to reconnect themselves after mechanical rupture during the mode I experiments. It is important to notice that during manufacturing of the samples, there is a diffusion of SP polymer into the epoxy matrix and consequently, the intra SP propagation of the delamination under mode I loading. Due to the sufficiently low viscosity of the SP polymer at 100°C, it flows along the crack flanks and covers the debonded surfaces. The presence of the thermally reversible hydrogen bonds between the polymer chains, anchored strongly on the crack flanks, under mechanical loading, facilitates the extensive contact between the SP polymer chains and the final rebonding upon cooling. The observed reduction in the P_{max} and the G_{IC} values with increasing number of healing cycles, is attributed to the progressive deactivation of the thermally reversible hydrogen bonds versus exposure time at high temperature and an uneven distribution of the SP film over the debonded surfaces during the healing cycle at 100°C, which concludes to thickness variation of SP polymer and variation of the delamination propagation locally.
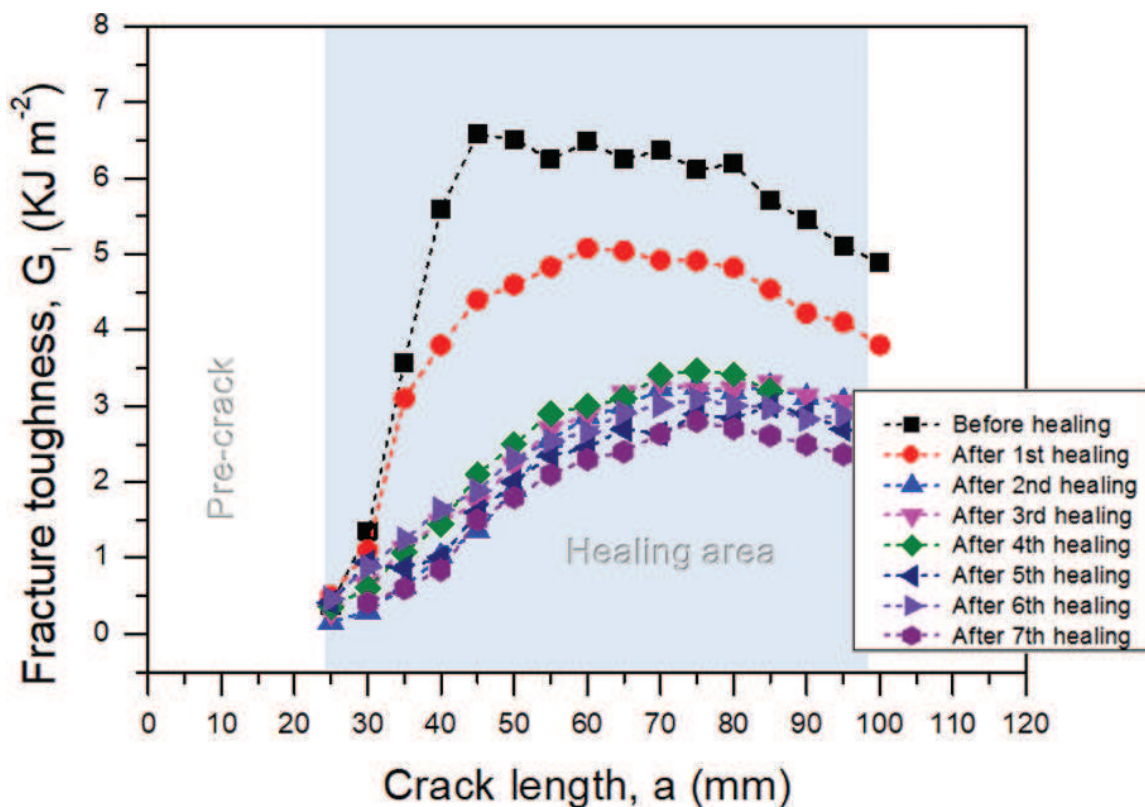

Figure 12. Representative R-curves of the modified composite before and after the healing cycles, showing the relation between G_I and crack length (a).

The typical R-curves under mode I loading conditions before and after the application of the healing cycles are depicted in **Figure 12**, and they are consistent with the load-displacement data. The general trend is that with increasing number of healing cycles, the G_{IC} values decrease and the plateau values of the G_{IC} reach at a slightly later stage than the corresponding plateau value of the pristine SP-modified interleaf composite, at 50 mm instead of 45 mm. In line with the pristine SP sample, the plateau value remains almost constant until a crack growth length of about 80 mm. It is necessary to stress that after the first rupture of the interleaf-modified composite, the only active material that works and keeps the upper and lower fractured surfaces together after healing activation, is the reversible polymer material and the epoxy matrix infiltrated by this. More information can be found in Ref. [33].

3.2.3. Knock-down effect on in-plane mechanical properties

The incorporation of the SP interleaf into composites laminate is expected to have an impact on in-plane properties of the composite. For this purpose, 3PB tests were conducted for the reference and the modified CFRPs, where a layer of SP polymer was placed at the middle surface of the composite. According to these experiments, it was shown that there was no knock-down effect on the flexural modulus (E_{flex}) of the composite as it was retained close to 55.5 GPa for both reference and modified CFRPs (due to the position chosen for the introduction of SP polymer). On the other hand, the flexural strength (σ_{max}) value was reduced by 22% (from approximately 638 to 493 MPa). Bar chart in **Figure 13** describes these results in detail. Based on this, a more detail investigation is needed for evaluating completely the effect of the introduction of SP polymers into the composite laminate.
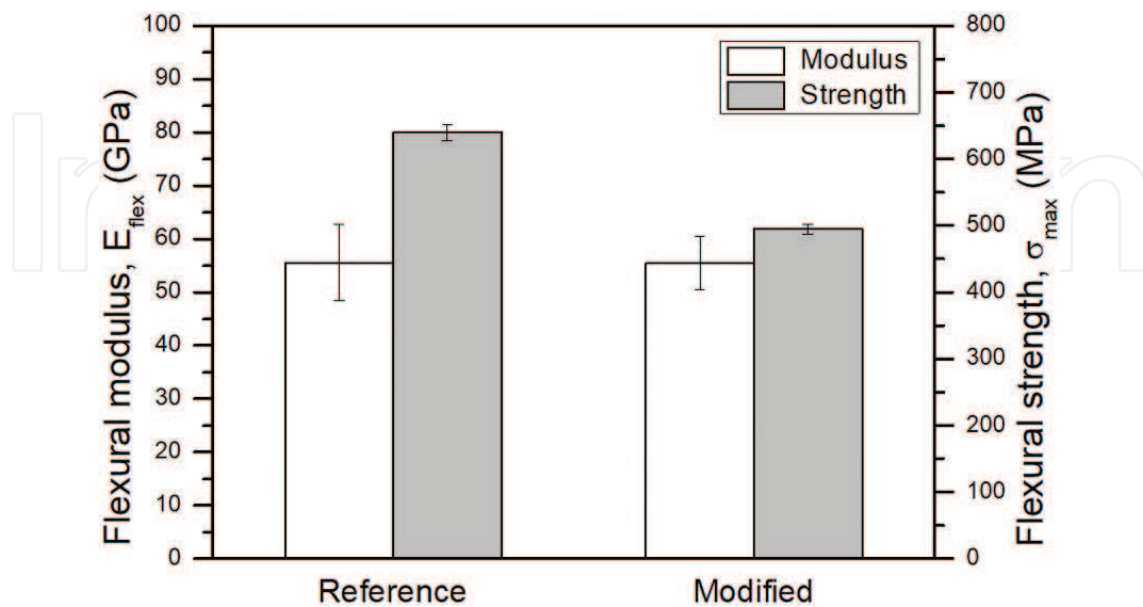

Figure 13. Knock-down effect of the SP interleaf on the E_{flex} and σ_{max} values of the CFRP.

4. Mode II interlaminar fracture toughening and healing of carbon fiber/epoxy composites by hydrogen-bonded supramolecular polymer interlayers as SHA

4.1. Composites manufacturing

Two UD laminated plates made of 22 prepreg layers were manufactured for the needs of the current study; the reference laminate and the modified laminate containing the SP interleaf on the mid-plane, both appropriate for deriving mode II interlaminar fracture specimens. **Figure 14** shows schematically the plate configuration with respect to the fracture pre-crack and the SHA location. During the manufacturing process, two 13-μm-thick sheets of PTFE film were placed in the mid-thickness plane of both laminates as shown in **Figure 14** to act as initial pre-crack according to the request of the interlaminar fracture test. In the case of the modified laminate, a SP strip was carefully placed on the mid-plane as shown in **Figure 14(b, c)**. Following the lay-up, the laminates were vacuum bagged and cured in autoclave for 2 h at 130°C under 6 bar pressure, according to the prepreg supplier guidelines. The dimensions of the plates were 300 mm × 150 mm × 3 mm. Five mode I (DCB) samples were cut from both the reference and the modified plate. The incorporation of the SP film in the mid-plane of the modified laminate did not appear to have a significant effect on the thicknesses of the samples. The fiber volume fraction of all manufactured plates was calculated to be close to 60%.
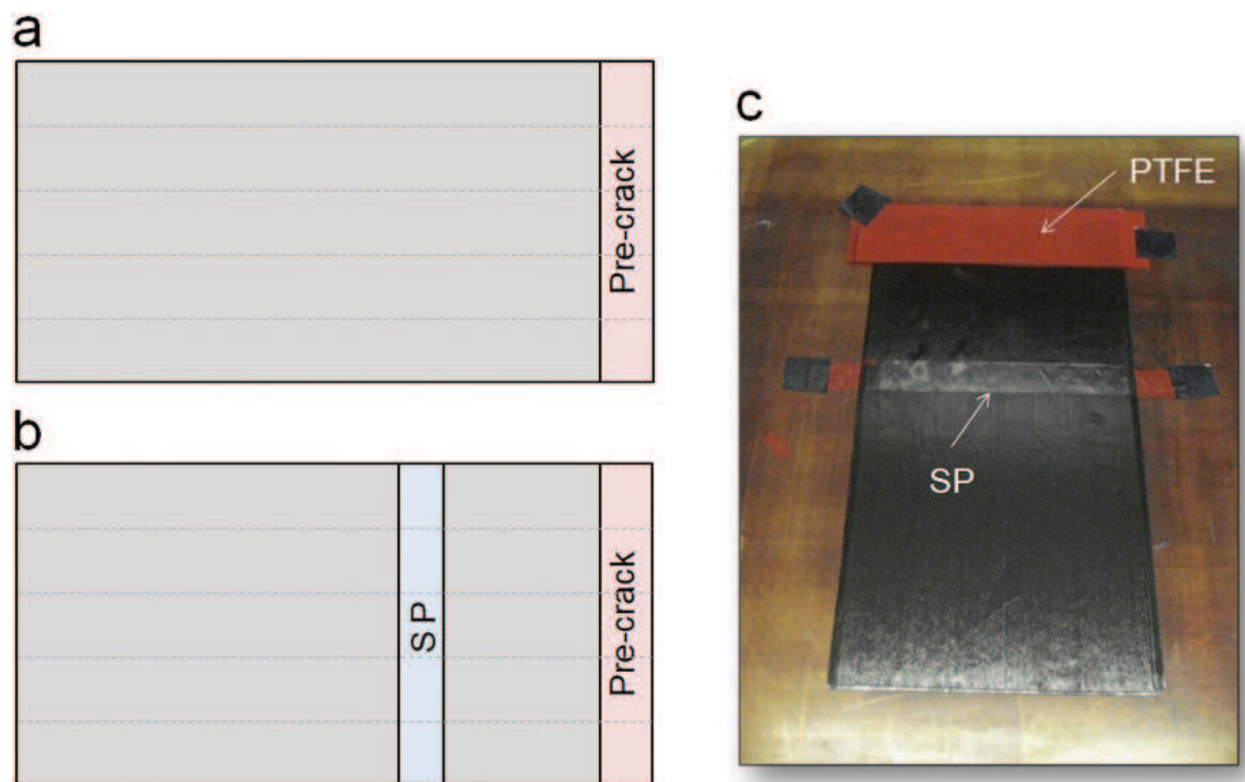

Figure 14. Schematic representation of the mid-plane of (a) the reference plate and (b) the SP containing modified plate. (c) Photograph of the mid-plane of the modified plate, where a SP strip was carefully positioned, together with the PTFE film.

4.2. Mode II interlaminar fracture toughness testing

The mode II experiments were performed according to specifications described in Section 2.1.4. Based on Eq. (2), the crack length (a) has to be known in order the G_{IIC} value to be calculated. For brittle materials, the moment of unstable crack growth can be clearly determined; P_{max} is attributed to the critical load at the onset of crack growth. On the other hand, for modified materials containing ductile interleaves in which the crack is growing through the ductile interleaved layer as described in Section 3, the crack initiation (P_{ini}) occurs long before P_{max}. In addition, in mode II loading of the pre-cracked specimen the crack tends to close which hinder a clear visualization of its tip. Thus, mode II fracture characterization of CFRPs with a ductile interlayer remains a major challenge including uncertainties on the results. **Figure 15**, depicts the modified ENF test specimen configuration as derived from DCB specimen.

Based on these, whereas in the case of reference CFRPs the G_{IIC} calculations were extracted directly from the P-d data without any concern, for the modified CFRPs the monitoring of the crack growth was carried out by using a high-resolution digital camera system **Figure 16**. It is suggested that the crack initiation point of the modified CFRPs corresponds to the onset of the visual deviation of linearity in P-d curves. In addition, a vertical line with pencil was marked at the end of the starter film, as shown in **Figure 16**. It is suggested that the separation of the line into two lines corresponds to the crack initiation.
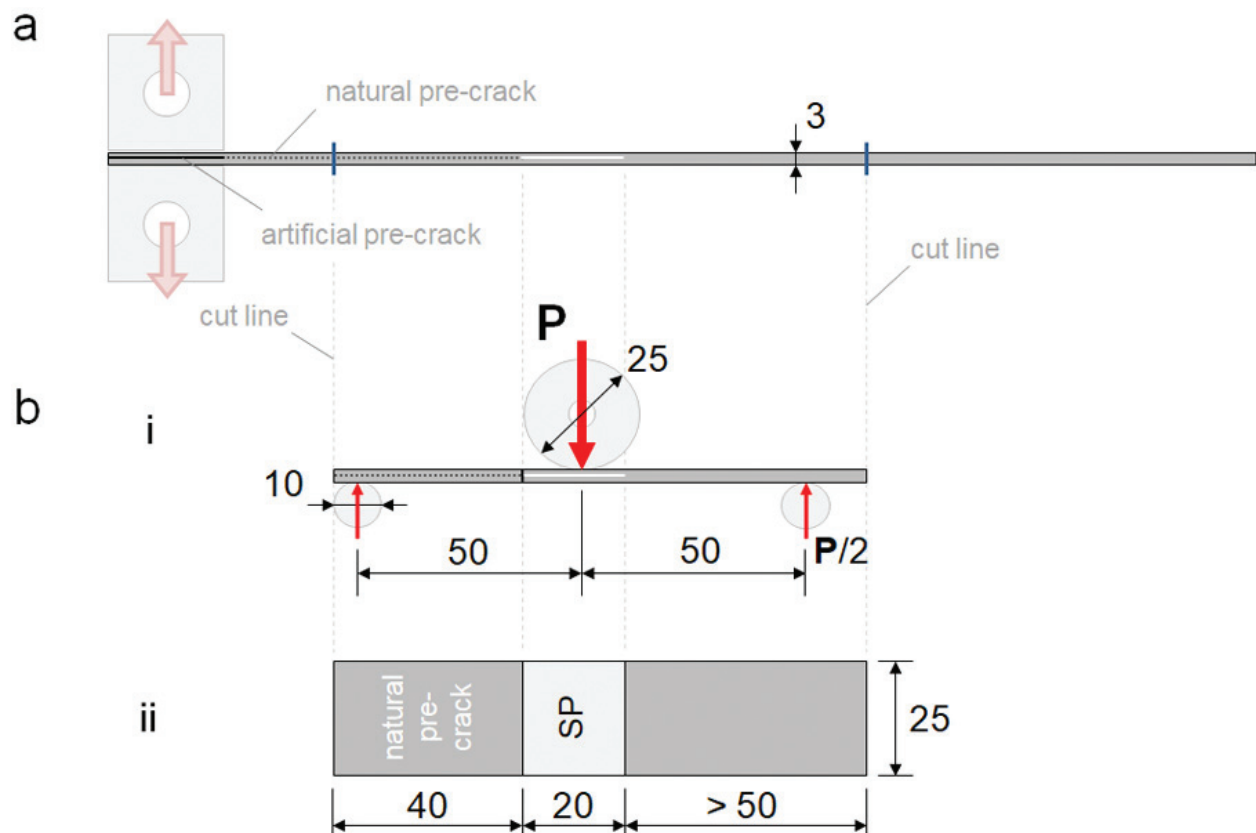

Figure 15. Schematic depiction of the modified ENF test specimen configuration as derived from DCB specimen. (a) DCB specimen, (b) ENF specimen, (i) side view, (ii) top view. Dimensions in mm.
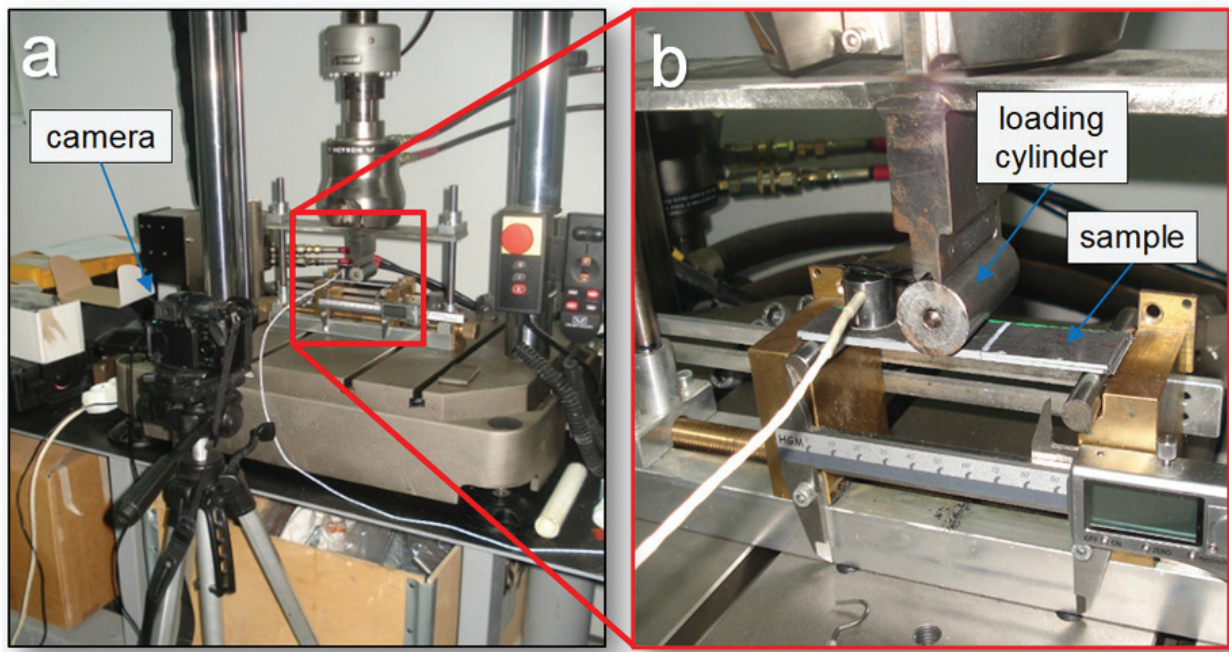
Figure 16. Experimental setup of the mode II interlaminar fracture toughness tests where the high-resolution camera monitoring of the crack evolution is seen.

4.3. Results and discussion

The study is deployed in two parts. The first part covers the assessment of the performance change due to the introduction of the SHA in the reference CFRP system. It is possible that the approach to introduce the healing functionality may jeopardize the load-bearing capacity of the composite. This change in performance is commonly referred to as the knock-down effect. The second part of this study deals with the healing functionality of the composite system and its performance. Essentially, once the SHA has been incorporated, the system is expected to have a healing functionality; meaning the capability to heal damage in the form of cracks (intrinsic or externally activated). The extent to which this functionality delivers its purposes is assessed in the second level of this work. Details on the procedure are given in the next paragraph.

4.3.1. Mode II fracture toughness: reference versus modified CFRP

The introduction of the SHA in the CFRP architecture is expected to have an impact on the material performance. At this part of the work the impact on mode II fracture toughness is assessed. The mechanical response of the reference and the modified CFRP to mode II fracture loading in combination with crack evolution camera recording was studied.

Typical load-displacement (P-d) curves for the reference and the modified plate are given in **Figure 17(a)**. All specimens within each set showed a similar behavior. The average values and standard deviation for the two material sets are shown in **Figure 17(b)**. As previously mentioned, the P-d behavior of the two material sets differs. For the reference material, the applied load increases linearly until the onset of the pre-crack propagation where the load drops abruptly. On
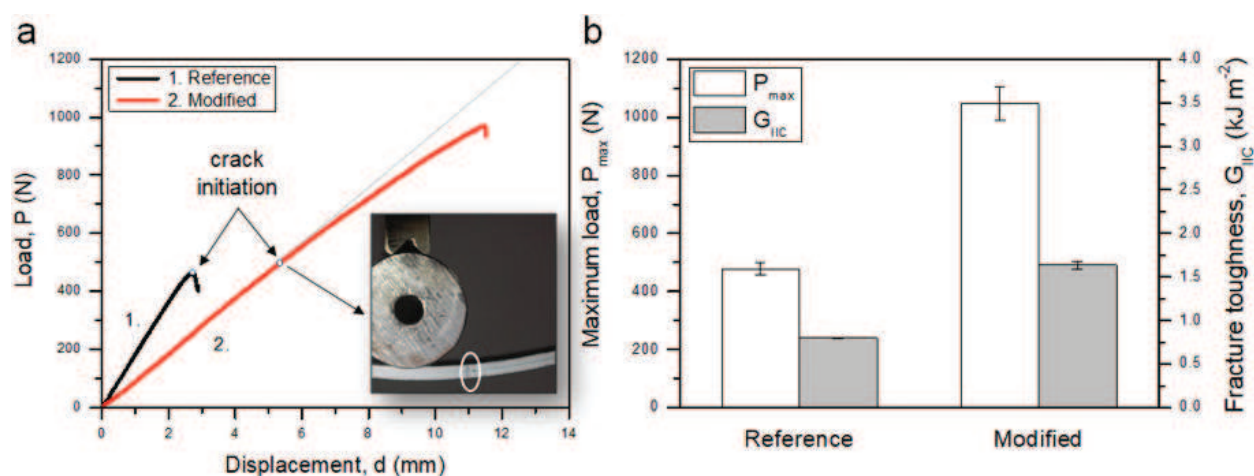
Figure 17. (a) Representative load (P) versus displacement (d) curves for the reference and modified CFRPs during the mode II interlaminar fracture toughness test. (b) Comparison between the reference and the modified CFRP, for the P_{max} and the G_{IIC} values, respectively.

the other hand, for the modified CFRP, the initially linear P-d relation is followed by a distinguishable deviation from linearity and much latter the load drop appears. Whereas the load drop for the reference case is attributed to the crack evolution onset, for the modified CFRP the P_{max} indicates the load-bearing capacity of the composite before undergoing major damages. Interestingly, the modified laminate exhibits a significantly higher P_{max} and respective displacement. As seen in the **Figure 17(a)**, P_{max} is more than double that of the reference CFRP (120% increase) while the displacement at failure is approximately four times larger than the reference.

From the recorded mechanical data, the mode II interlaminar fracture toughness (G_{IIC}) was calculated. For the calculation, the displacement (d) at crack propagation onset is needed to be known. The crack initiation points for the reference and the modified CFRP, determined as described in Section 4.2, are marked in **Figure 17(a)**. The snapshot of **Figure 17(a)** corresponds to the marked crack initiation point for the modified specimen. In this snapshot, a slight separation of the pencil line into two lines is observed. The G_{IIC} for both material sets were calculated using in Eq. (2) the (P, d) values that correspond to the indicated points of the curve. The average values and standard deviation are shown in **Figure 17(b)**. The G_{IIC} values for the modified CFRP exhibit an increase of 100%, which is related both to the slightly higher corresponding load (P) recorded and to the displacement (d) at that instance.

The post-tests inspection revealed the in-plane crack propagated through the SP interleaf rather than along the SP-epoxy interface. This observation indicates that the interface of the interleaf to the host matrix is stronger than the properties of the interleaf, thus guiding the crack to a lower energy path through the interleaf (see Section 3). This was also monitored in the case of mode I experiments. This behavior essentially maximizes the effectiveness of the interleaf and explains the higher resistance to crack propagation. In addition, high displacements are recorded while the load increased steadily. This can be related to the ductile behavior of SP polymer, in combination with its strength. Even when the crack initiated, the presence of the SP interleaf arrests the crack and prevents propagation due to the developed shear bridging (see Section 3) within the crack sides. These results to lower stress at the crack tip

and consequently to an increased mode II interlaminar fracture toughness. Based on these results, it is clearly shown that the presence of the SP interleave in the composite resulted in a considerable increase of the mode II interlaminar fracture toughness characteristics. On the other hand, the mechanisms delivering this increase of mode II fracture toughness are related both to the SP-epoxy interface (the diffusion of SP polymer into epoxy matrix), as well as the structural properties of the interleaf itself. Thus, it is obvious that the fracture toughness characteristics of the composite have been enhanced significantly by the introduction of the SP interleaf. It can be concluded that, regardless of the healing functionality performance, this finding is extremely positive and of great interest.

4.3.2. Assessment of healing functionality of composites

The healing functionality of these SP interleaves into CFRP composites was assessed by subjecting the samples to a healing cycle consisting of heating and compression as described in Section 2.1.7. Indeed, a large recovery of the interlaminar characteristics (P_{ini}, P_{max} and G_{IIC}) during the repeated mode II experiments was observed when the fractured samples had been subjected to multiply healing cycles.

In **Figure 18(a)**, the recorded load-displacement data are shown for a representative modified CFRP specimen. There are five curves; one for the initial test (before healing) and one after each consecutive healing cycle. In all curves, the general trend is the same; the initially linear P-d part of the curve is followed by a deviation from linearity. In subsequent healing cycles, the sample exhibits a drop in stiffness as well as a smaller P_{max} value. Nevertheless, the lowest P_{max} value remains well above that of the reference value (approximately 80% higher). In **Figure 18(a)**, a magnification of the curves at the crack initiation points is given and for each curve the crack initiation points are marked. In the histogram of **Figure 18(b)**, the effect of the number of healing cycles on the mode II fracture characteristics (P_{ini}, P_{max} and G_{IIC}) of the modified CFRP is presented. After the first healing activation, the P_{ini} and P_{max} values of the modified CFRP showed a decrease of approximately 5 and 16%, respectively. The same decreasing trend was observed also after the second healing cycle when the values are compared against the values concluded after the first healing cycle. Following the third healing cycle the decrease of the P_{ini} and P_{max} values were much lower, this was also the trend after the fourth healing cycle. On the other hand, the G_{IIC} values appear a slight increase with increasing the number of healing activation cycles; the G_{IIC} value after the fourth healing cycle is 14% higher than that achieved by the initial SP-modified CFRPs. This behavior is attributed to the fact that the displacement value at crack propagation onset increases as the healing cycles increase (see Eq. (2)). In **Figure 18(c)**, the actual HE values for the three quantities of interest (namely G_{IIC}, P_{ini} and P_{max}) calculated based on Eq. (3), are given as a function of the number of healing cycles. In subsequent healing cycles a drop for the HE_{Pini} and HE_{Pmax} is observed. Nevertheless, the lowest value remains over 70% of the reference values of pristine CFRPs. On the other hand, the bending stiffness of the modified laminate presents a gradual decrease with increasing the number of healing activations.

The partial recovery may is associated with the degradation of the SP properties, as well as the epoxy-SP interface after each loading/healing cycle. In addition, the interlaminar cracked area is only partially healed after the subsequent healing cycles. Snapshots of the sample during the mode II experiments at the crack initiation and fracture points before and after the healing
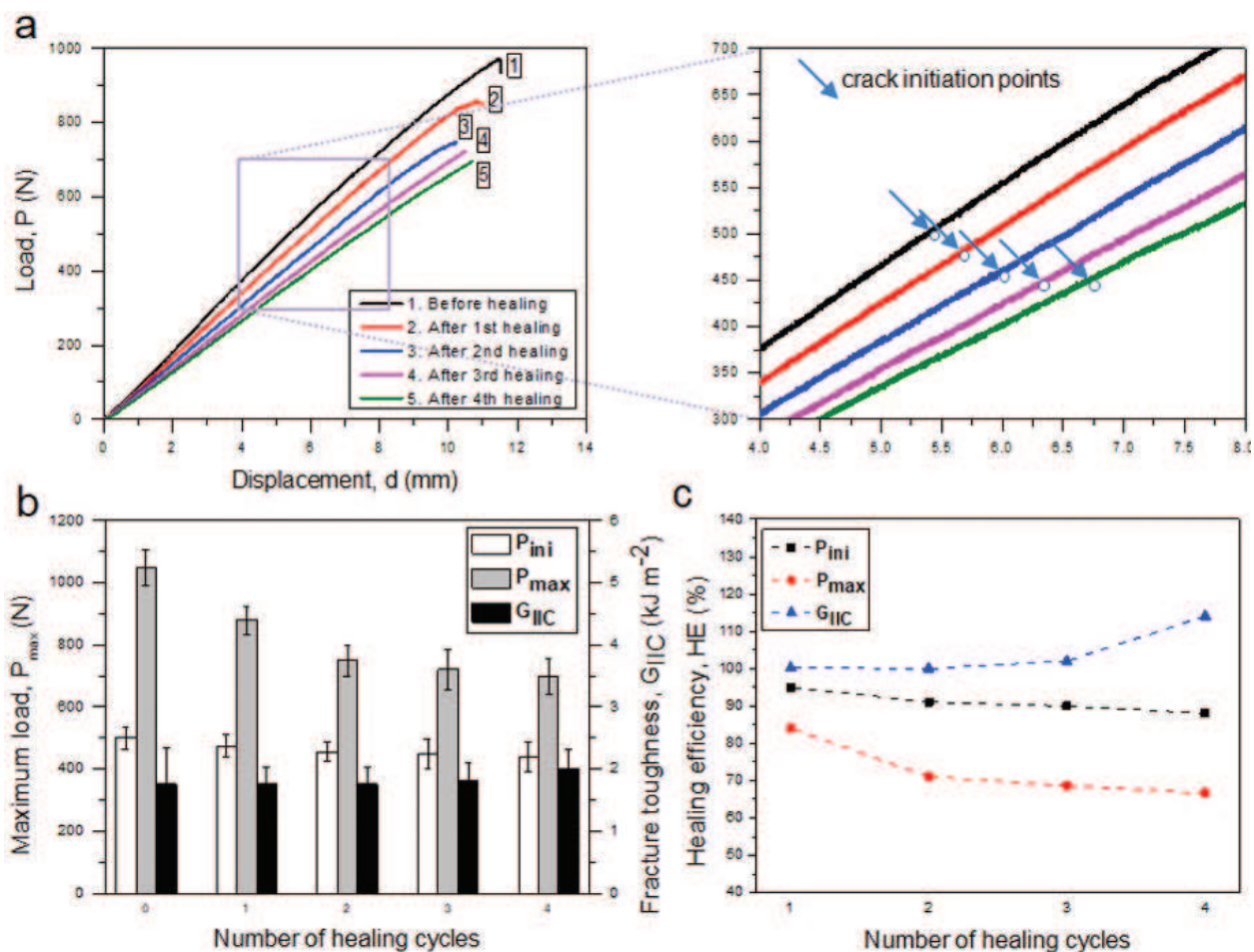
Figure 18. Results from the mode II interlaminar fracture toughness tests of the modified CFRPs before and after four healing cycles. (a) Representative load (P) versus displacement (d) curves for the modified CFRP before and after the healing cycles and determination of the crack initiation point. (b) Bar diagrams for the P_{ini}, P_{max} and G_{IIC} values of the modified CFRP, before and after the healing cycles. (c) The effect of the number of healing cycles on the HE of the modified CFRP, in terms of the P_{ini}, P_{max} and the G_{IIC}.

cycles are illustrated in **Figure 19(a)**. The high HE proportions and the ability of the SP interleaf to heal the cracks are attributed to the SP material's chains that can reconnect themselves after the mechanical rapture during the mode II experiments. Critical parameters are a good coverage of the fractured surfaces by the SP material and a sufficiently low viscosity of the reversible polymer at 100°C in order to be able to flow into the crack flanks and to reposition itself equally over the debonded surface. Therefore, the observed reduction in the P_{max} value with increasing number of healing cycles can be attributed further of the degradation of SP material, to an uneven spreading of the SP interleaf over the fracture surface during the healing cycle. An important point to note is the observation that the apparent flexural stiffness of the system decreases after multiple healing activations. Several reasons have been identified to answer to this observation. Firstly, the tests extended to very large deformation which can lead to the breakage of the fibers on the outer layers. As a matter of fact, **Figure 19(b)** shows evidence of broken fibers on the loading cross-head side. It is proposed that these excessive damages were reflected as portion reduction in the load versus displacement curve. Secondly, during the SHA activation it is possible that not all the interface surface of the crack is healed. Thus, the system
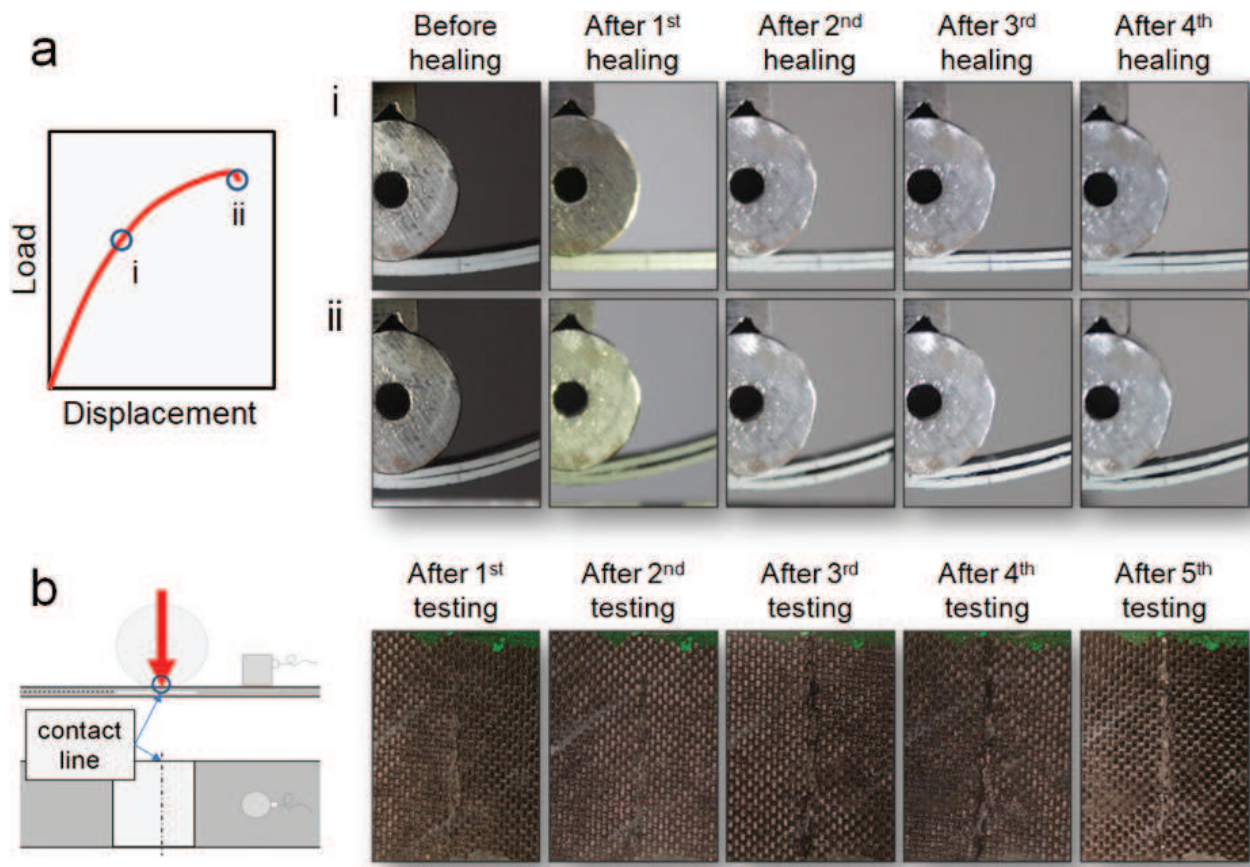
Figure 19. (a) Snapshot during the mode II interlaminar fracture toughness testing of the modified CFRP (i) just after crack propagation onset and (ii) just before failure (i.e. $P \sim P_{max}$), before and after healing. (b) Photographs showing the progressive damage accumulation on the upper layers of the modified CFRP during the mode II testing, with increasing the number of testing cycles. The damaged line is the contact line between the specimen and the loading cylinder.

cannot recover the initial stiffness since the extent of the delamination is larger. Finally, the healing functionality of the SP may degrade after multiple activations; an observation also noted in Section 3 with the same material. According to this work, the bulk SP material can withstand at least seven healing cycles with excellent healing recoveries (still higher toughness values compared to the reference one), but in the present case of mode II loading the experiments were stopped after the fourth loading/healing cycle. The post-testing examination of the fracture surface of the healed laminates revealed that the SHA was clearly separated between the two adjacent fracture surfaces. Thus, the healing effect of the SP material was fully utilized. More information can be found in Ref. [34].

5. Low-velocity impact response and compression after impact assessment of carbon fiber/epoxy composites containing hydrogen-bonded supramolecular prepregs as SHA

5.1. Composites manufacturing

Two types of quasi-isotropic laminated plates containing 16 plies, with $[45/0/-45/90]_{2S}$ stacking sequence each were manufactured for the needs of the current study; the reference laminate,

and the modified laminate, with two SP prepregs placed symmetrically into the composite. Both material groups (reference and modified) were tested under compression prior of impact, in order to identify possible knock down in compression strength. After exposed to LVI, CAI tests were performed for the pristine CFRP plates as well as for the SP prepreg modified ones, but in this case before and after the application of the healing activation cycle. **Figure 20**, shows schematically the configuration of the plates (**Figure 20(a)**) and the position where the two SP prepregs were placed (**Figure 20(b)**). The SP prepregs replaced the 6th and 11th UD 90° layers of the composite (**Figure 20(b)**). Following the lay-up, the laminates were vacuum bagged and cured in an autoclave for 2 h at 130°C under 6 bars applied pressure, according to the prepreg manufacturer guidelines. The dimensions of the final plates were 150 mm × 100 mm × 2.1 mm. Ten reference and 15 modified impact test samples were manufactured, respectively. Five samples of pristine CFRPs and 10 samples of SP prepreg-modified CFRPs were exposed to impact tests. All the samples were tested to CAI. In the case of SP prepreg-modified samples one group was tested to CAI just after initial impact, while a second group was passed through a healing cycle (following the earlier described cycle) and after this step they were also tested to CAI.

5.2. Results and discussion

5.2.1. Composites manufacturing

The handling of the CF/SP prepreg plies at RT and the incorporation of them into composite laminate did not create any concerns. SP prepreg seem to combine characteristics of both traditional thermoplastics (good processability, softening and flow at elevated temperatures). The modified prepreg UD plies had an average thickness of 180 μm each and thus they did not alarmingly thicken the entire CFRP laminate. The fiber volume fraction of both composite groups was calculated to be slightly lower for the modified plates (approximately 60% for the reference while approximately 59% for the modified ones, respectively). They also did not disrupt the fiber architecture. In **Figure 21**, optical microscopy cross-section photographs of reference and modified CFRPs with SHA based on SP are illustrated. Optical microscopy photograph of the modified CFRPs show the location where the SHA has been incorporated symmetrically.
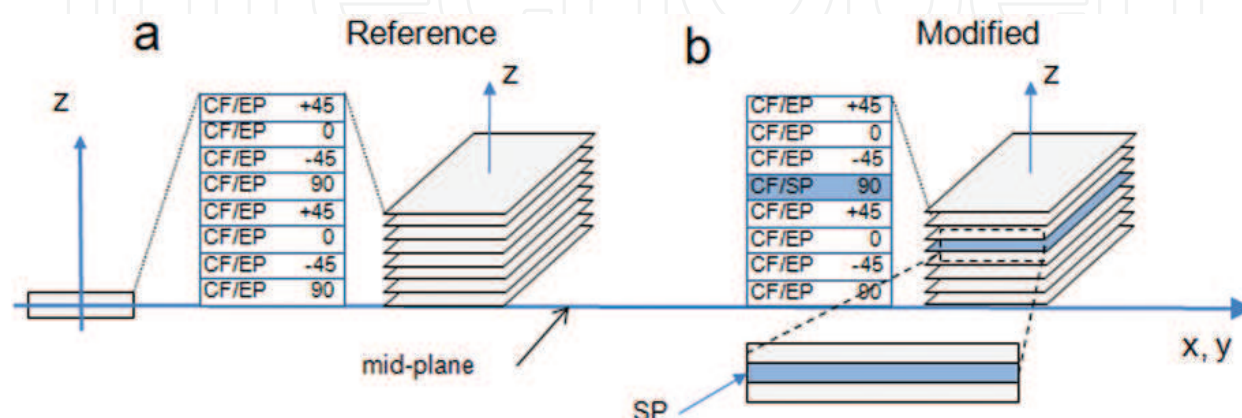

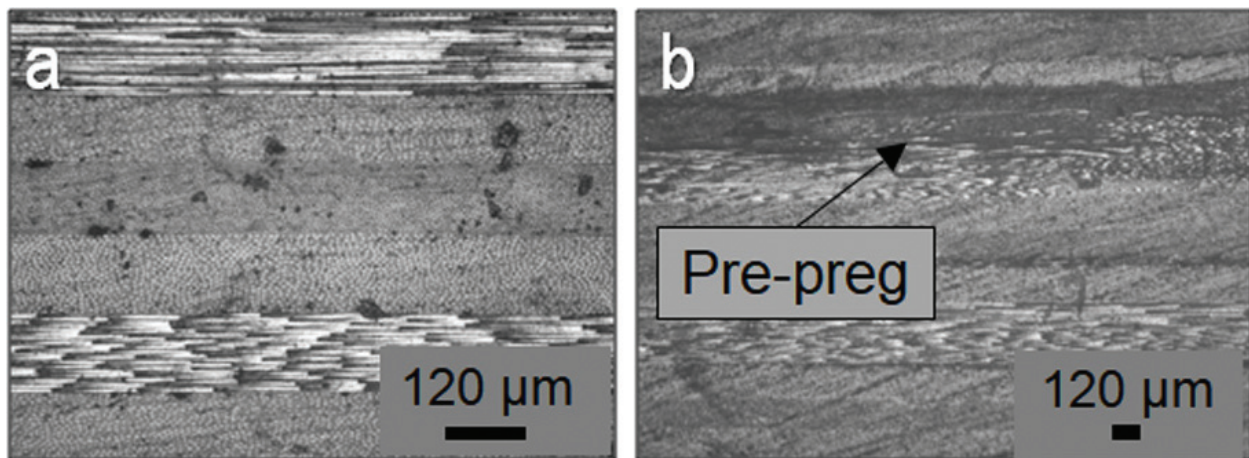**Figure 20.** Design of (a) the reference CFRP, (b) the modified CFRP with SP prepregs.

Figure 21. Optical microscopy photographs of (a) the cross-section area of reference CFRPs, (b) the cross-section area of modified CFRPs with SP prepregs in which the SHA area is also clearly illustrated.

5.2.2. Resistance to low-velocity impact

Reference and modified CFRPs were subjected to LVI as described in Section 2.1.5. After testing, C-scan inspection measurements were performed to evaluate the impact-induced damage. The typical C-scans for all material types in the before and after impact situations are shown in **Figure 22(a, b)**. The white region in the center of the images in **Figure 22(a, b)** represents the damage area (mainly delamination) induced by the impact event. For the determination of the impact damage area, post-processing software was utilized. The software was able to quantify the white region area (damage area) of the recorded C-scan images after the LVI event for both material sets. These areas were calculated to be approximately 592 and 115 mm^2 for the reference and the modified plates, respectively. Thus, the modified composites exhibit higher resistance to delamination, compared against the reference ones. The incorporation of the SHA in prepreg form into composite laminate increases the LVI damage resistance of the final material. The SP prepreg provides higher energy absorption characteristics to the entire composite due its ductile nature, during LVI. In the present work impact energy of 25 J was used. It is considered a moderate amount of impact energy that does not occurs fiber breakage and the main damage mode that is promoted is delamination. In fact, no visible or detectable damage was shown on the top and bottom faces of the reference samples after LVI testing. On the contrary, optical inspection of SP-modified prepreg samples exhibited only indentation on the top face (**Figure 22(ci)**), while no ply splitting phenomena were observed on the bottom face of the CFRP plate (**Figure 22(cii)**).

In general, during an impact event with moderate impact energy, the impact energy introduced into the composite structure is mainly absorbed through elastic deformation and through different failure modes. In CFRPs, plastic deformation does not take place. Samples containing SHAs with a ductile nature such as SP, plastic deformation takes place. **Figure 23** illustrates cross-section photos at the center of reference and modified CFRPs (around the impact site) after LVI. According to **Figure 23(a)**, the formation of multiple delaminations sites in the reference sample is apparent. On the contrary modified CFRPs exhibited different
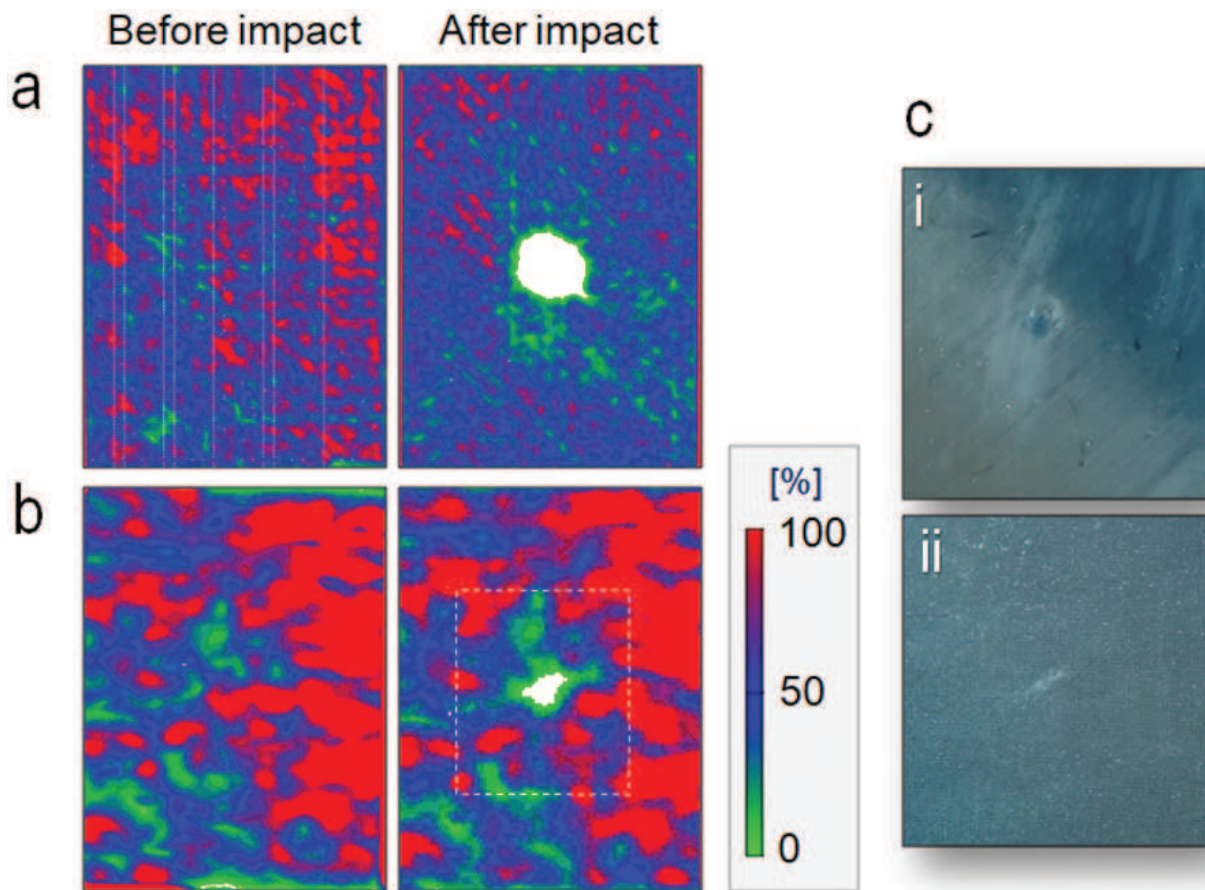
Figure 22. Representative C-scan inspection images of the (a) reference CFRP, (b) modified CFRP with SP prepregs in the before and after the LVI situation. (c) Indicative top- and bottom-face photographs after LVI for the SP prepreg-modified composites.

behavior after LVI. Extended damage has been occurred into the composite in the form of delaminations and significant transverse cracks that leads to off axis ply split.

5.2.3. Repair of the impact-induced damages via the healing treatment

After LVI tests, one group of the SP prepreg-modified samples were subjected to heating under controlled through-the-thickness compression as described in Section 2.1.7. After healing, C-scan was performed in order to evaluate the reduction of the impact damage in the areas where the SP prepregs have been placed. Interestingly, it was found that after healing the modified samples exhibited macroscopically a HE of about 40% (accounting by the measurement of the impact damage area before and after healing, as it demonstrated globally in the C-Scan plots (**Figure 24(a**, right)).

The HE value was calculated according to Eq. (4). Modified composites were not able to heal the entire damage after the healing process as **Figure 24** suggests. The SHA has the trend to follow the carbon fibers (90° ply). This behavior was also validated by optical microscopy examination of the damaged samples after the healing process. Materials micro-structure examination under optical microscopy was used to validate the results from non-destructive
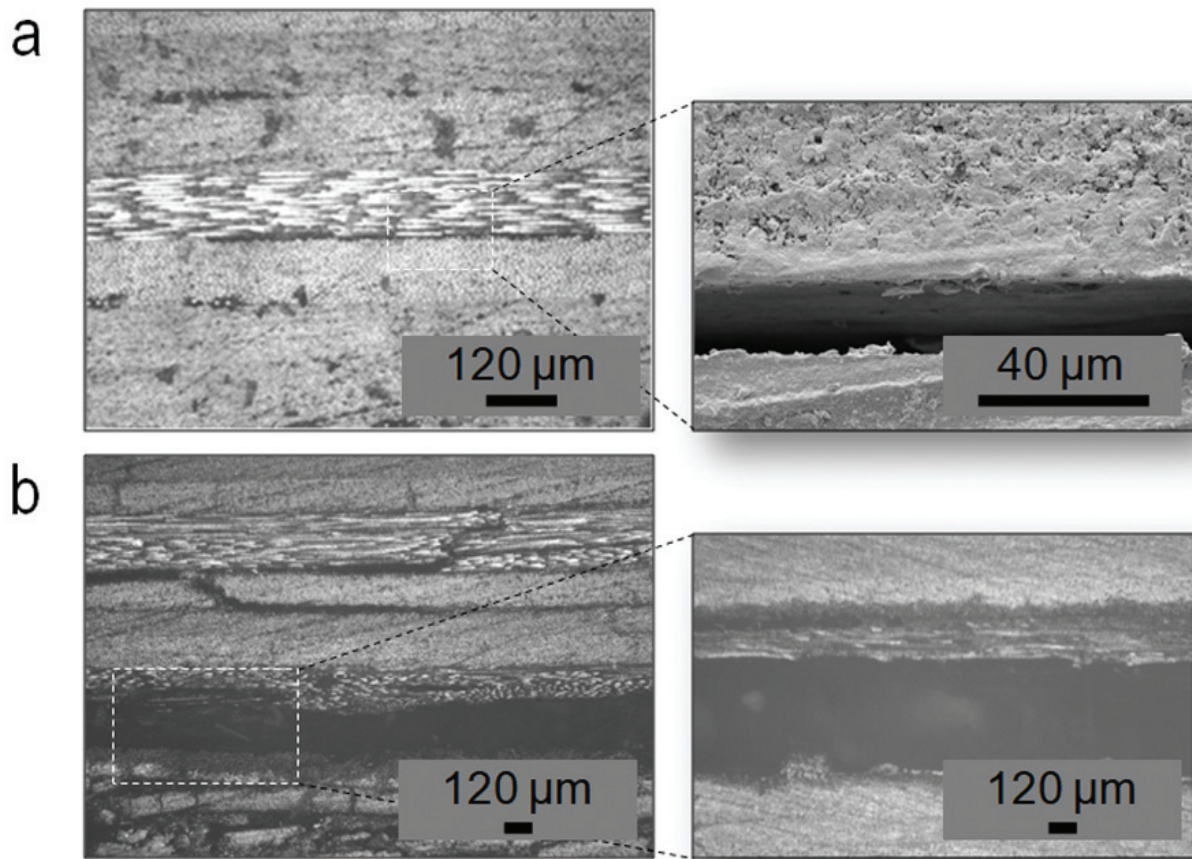
Figure 23. Optical microscopy photographs for reference and modified CFRPs cross sections after LVI situation (a) reference CFRP, (b) modified CFRP with SP prepregs.
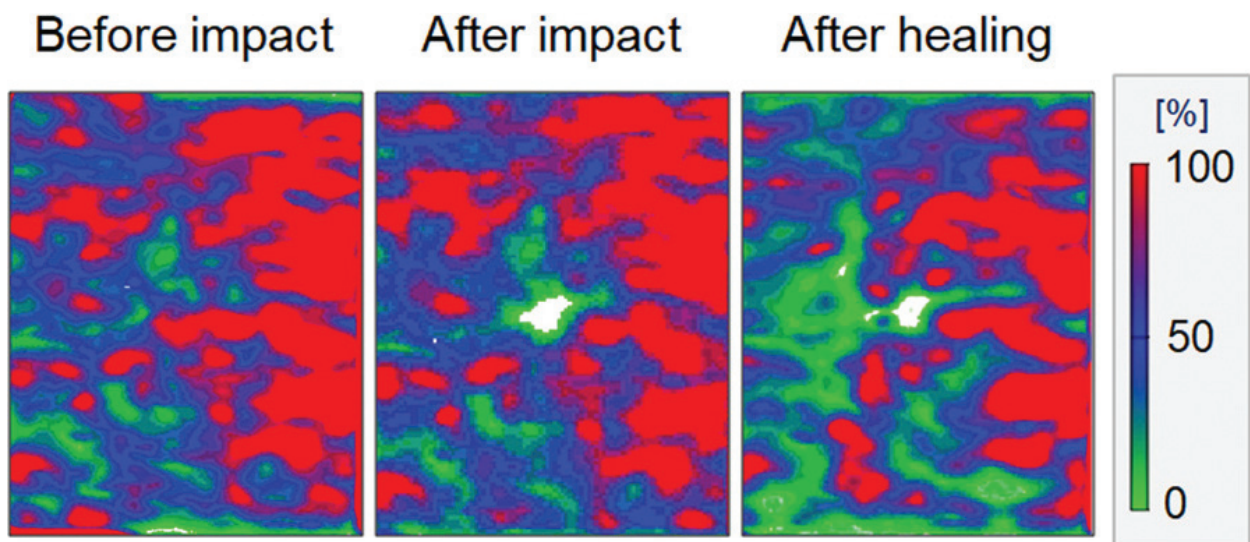

Figure 24. Representative C-scan inspection images of the modified CFRP plates with SP prepregs, in before, after impact situation and after healing process.
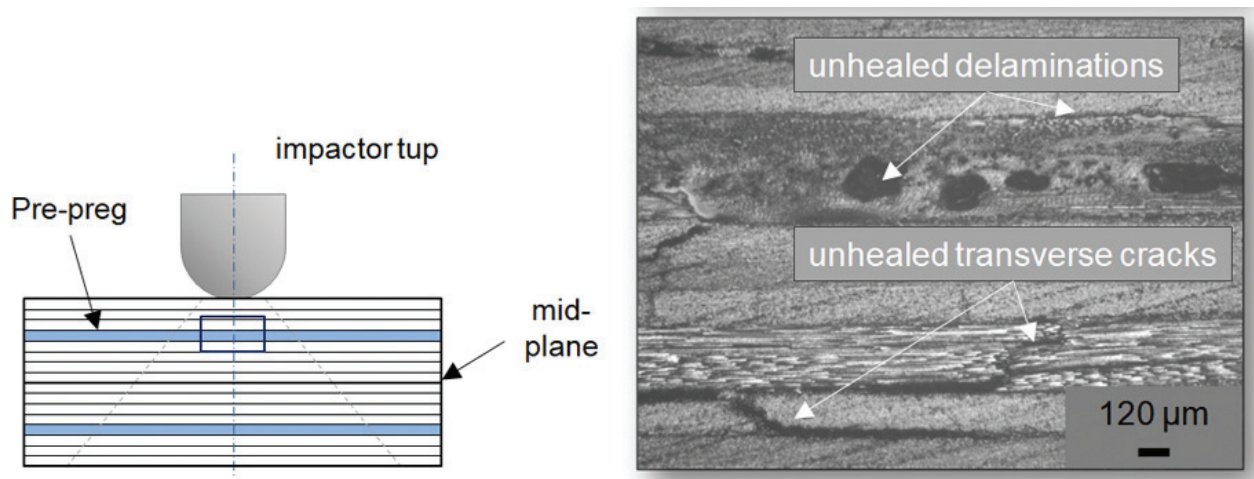
Figure 25. Optical microscopy photograph of the SP-modified CFRP cross section after the healing process.

C-scan inspections. In **Figure 25**, the optical microscopy photos of the cross sections of the repaired modified CFRPs are illustrated. **Figure 25** zooms in the SHA area (CF/SP prepreg layer) and the upper and lower adjacent layers of the laminate. For the modified samples (**Figure 25**) the presence of many delaminations after the healing process is still apparent, as it is expected in all the interfaces that do not contain SP material. Only areas adjacent to SP were healed and this is the reason why low HE value for the damaged area in modified samples was achieved.

5.2.4. Compressive behavior of CFRPs before impact

The incorporation of SP prepreg into composite laminate is expected to have an impact (i.e., knock-down effect) on final composites' mechanical performance. In the present subsection, the effect on the compressive properties is assessed. Typical stress versus strain curves under compression before impact (CBI) for the reference and modified CFRPs (unimpacted) are illustrated in **Figure 26(a)**. In all curves, the initially linear stress versus strain response is
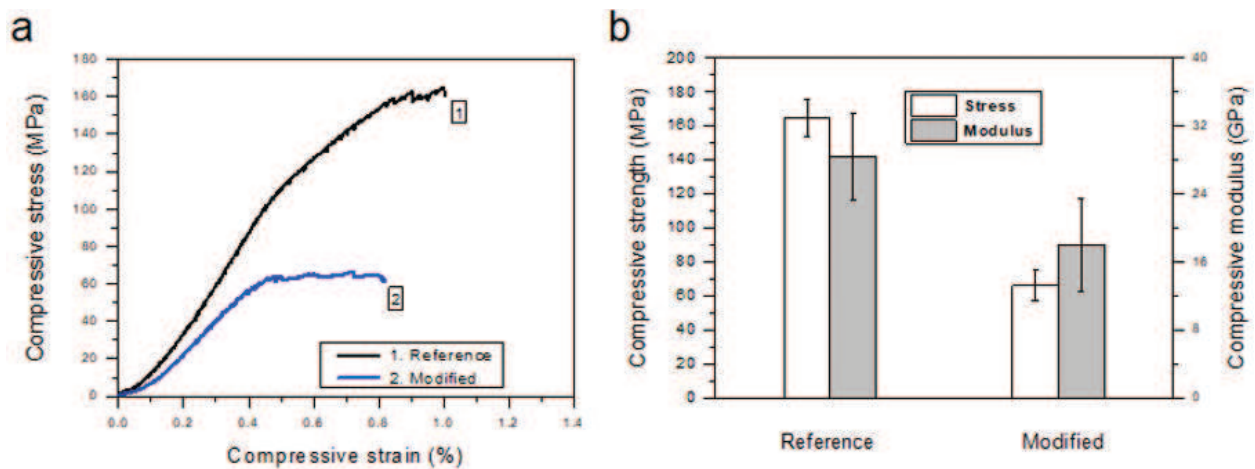

Figure 26. (a) Representative compressive stress versus compressive strain (%) curves from the CBI testing of the reference and modified CFRPs. (b) σ_{max} and E_{comp} the values of the two material types.

followed by a deviation from linearity and load drop just before the end of the test. The compressive strength (σ_{max}) and the effective compressive modulus (E_{comp}) values of the two material types are summarized in **Figure 26(b)**. Modified CFPRs exhibited lower compression characteristics than the reference ones. The σ_{max} was decreased by 60% whereas E_{comp} by 55% due to SP SHA introduction. Thus, even though SP prepreg promotes the energy absorption under out-of-plane impact loading, it adversely deteriorates the in-plane (compressive) properties of the final CFRP.

5.2.5. Residual compressive properties of the CFRPs after LVI

As already described, after LVI tests reference and SP-modified samples were loaded in compression to assess their CAI properties. Also, the introduced healing functionality of the SP-modified samples was quantified by subjecting these samples to a simple healing cycle as described in Section 2.1.7 and then, repeating the CAI tests in order to investigate the post-healing CAI performance of the modified plates.

Typical compressive stress versus compressive strain (%) curves after LVI for reference and SP-modified samples (prior and after healing) are illustrated in **Figure 27(a)**. In addition, σ_{max} and E_{comp} values of both the reference and modified CFRPs in prior impact, after impact and after healing situation are summarized in **Figure 27(b)**. According to these results, it is shown that after LVI, the σ_{max} of the reference samples was reduced by 16%. SP modified samples, exhibited also the same reduction (16%) for the σ_{max} value. The reduction of the apparent compressive modulus (E_{comp}) is 5% for the reference and 9% for the SP-modified CFRPs. Furthermore, the SP-modified samples passed through healing process as it is has been already described earlier, and after that they exposed to CAI tests in order the post-healing performance of the composite plates to be investigated. According to these tests, it was shown that healed samples presented higher σ_{max} and E_{comp} values approximately 6 and 42%, respectively compared against the unhealed SP-modified ones (impacted samples). Therefore, modified samples improved CAI properties via healing treatment.
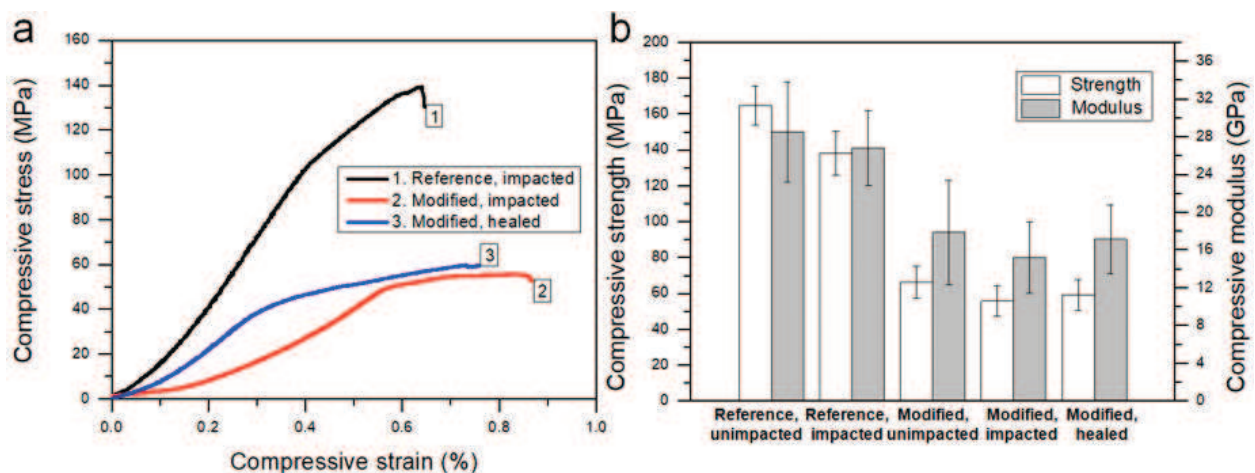

Figure 27. (a) Representative compressive stress versus compressive strain (%) curves from the CAI testing of both the reference and modified CFRPs (prior and after healing). (b) σ_{max} and E_{comp} values of both the reference and modified CFRPs prior impact, after impact and after healing.

As previously mentioned, the SP SHA was not able to heal all the cracks in the through-the-thickness direction. Only delaminations in the adjacent interfaces to the SP-modified ply were healed. After healing process, samples containing SP prepregs showed better load transfer characteristics. Finally, it is of note that whereas reference composites fail in a brittle manner, SP-modified CFRPs fail in a ductile or less brittle manner, both the virgin and healed ones. It is suggested that this result is a reflection of the ductile nature of the SP and of the softening effect induced by the presence of this type of plies as SHA into composites' architecture.

6. Outlook

The self-healing technology described in this chapter is envisioned to be incorporated locally in the early failure regions and other highly stressed areas of aeronautical CFRP structures. Also, this self-healing technology based on reversible polymers can be placed in known critical regions of structures where the damage predominately occurs, such as around drilled holes or on skin-stringer run-outs. These regions will take advantage of these repair mechanisms and do not represent the overall host matrix mechanical performance due to the knock-down effect of these polymers to the whole composite. It is obvious that the current tests do not represent the "real life service" conditions of these materials; however, this investigation demonstrates the self-healing capabilities of SP polymers. This preliminary "model study" proves the viability of the concept of incorporating the current SHAs into epoxy CFRPs.

7. Conclusions

In this chapter, the effect of the SP interleaf on the mode I and mode II interlaminar fracture toughness, as well as on LVI, CAI of CFRPs, and the provided healing capability was studied. SP polymer interlayers were locally incorporated into the area that the crack is expected to propagate. According to experimental results, it was shown that SP was able to considerably enhance the mode I and mode II interlaminar fracture toughness of the composites laminates through toughening and extended bridging. Characteristic example is G_{IC} value that was increased by more than one order of magnitude (1550%). These modified samples also exhibited high fracture performance recovery after first fracture for both mode I and II interlaminar fracture toughness. Potential knock-down effects on the in-plane properties of these modified samples were assessed. 3PB experiments revealed that by the incorporation of the SP interleaf into mid-thickness area, the ultimate stress (σ_{ult}) value was significantly decreased.

For the assessment of LVI behavior of CFRPs, SP prepregs were fabricated in order to the incorporation of the SHA into the composite to be simplified. Samples containing SP prepregs were examined under LVI and CAI tests and compared. Initially, it was shown that by the incorporation of the SP into composites laminate, the compression properties of the CFRPs were decreased. After LVI tests, samples containing SP prepregs exhibited higher resistance to damage, if compared against the reference ones. Healing process revealed that SP SHA was

not able to fully restore, even locally, the damage into the composite. Even though 100% healing was not achieved, SP prepreg-modified samples exhibited slightly improved compression characteristics after healing cycle.

Acknowledgements

Author details

Vassilis Kostopoulos* and Athanasios Kotrotsos

*Address all correspondence to: kostopoulos@mech.upatras.gr

Applied Mechanics Laboratory, Department of Mechanical Engineering and Aeronautics, University of Patras, Greece

References

[1] Ashby MF. Technology in the 1990s: Advanced materials and predictive design. Philosophical Transactions of the Royal Society of London. 1987;**332**:393-407. DOI: 10.1098/rsta.1987.0059

[2] O'Brian TK. Towards a damage tolerance philosophy for composite materials and structures. Composite Materials: Testing and Design, ASTM special technical publication. 1990;**1059**:7-33. DOI: 10.1520/STP24105S

[3] Wisnom MR. The role of delamination in failure of fibre-reinforced composites. Philosophical Transactions of the Royal Society A. 2012;**370**:1850-1870. DOI: 10.1098/rsta.2011.0441

[4] Blaiszik BJ, Kramer SLB, Olugebefola SC, Moore JS, Sottos NR, White SR. Self-healing polymers and composites. Annual Review of Materials Research. 2010;**40**:179-211. DOI: 10.1146/annurev-matsci-070909-104532

[5] Mezzenga R, Boogh L, Manson J. A review of dentritic hyperbranched polymer as modifiers in epoxy composites. Composites Science and Technology. 2001;**61**:787-795. DOI: 10.1016/S0266-3538(01)00022-7

[6] Masters JE. Improved impact and delamination resistance through interleaving. Key Engineering Materials. 1989;**37**:317-348. DOI: 10.4028/www.scientific.net/KEM.37.317

[7] Stevanovic MM, Stecenko TB. Mechanical behaviour of carbon and glass hybrid fibre reinforced polyester composites. Journal of Materials Science. 1992;**27**:941-946. DOI: 10.1007/BF01197646

[8] Dransfield KA, Jain LK, Mai YW. On the effects of stitching in CFRPs–I. Mode I delamination toughness. Composites Science and Technology. 1998;**58**:815-827. DOI: 10.1016/S0266-3538(97)00229-7

[9] Gilbert EN, Hayes BS, Seferis JC. Interlayer toughened unidirectional carbon pre-preg systems: Effect of preformed particle morphology. Composites Part A: Applied Science and Manufacturing. 2003;**34**:245-252. DOI: 10.1016/S1359-835X(02)00141-0

[10] Mouritz AP. Review of z-pinned composite laminates. Composites Part A: Applied Science and Manufacturing. 2007;**38**:2383-2397. DOI: 10.1016/j.compositesa.2007.08.016

[11] Chan WC. Design approaches for edge delamination resistance in laminated composites. Journal of Composites, Technology and Research. 1991;**13**:91-96. DOI: 10.1520/CTR10212J

[12] Chan WC, Ochoa OO. Edge delamination resistance by a critical ply termination. Key Engineering Materials. 1989;**37**:285-304. DOI: 10.4028/www.scientific.net/KEM.37.285

[13] Choi J, Yee AF, Laine RM. Toughening of cubic silsesquioxane epoxy nanocomposites using core-shell rubber particles: A three-component hybrid system. Macromolecules. 2004;**37**:3267-3327. DOI: 10.1021/ma0303723

[14] Howard WE, Gossard T Jr, Jones RM. Composite laminate free-edge reinforcement with U-shaped caps part II: Theoretical-experimental correlation. AIAA Journal. 1989;**27**:617-623. DOI: 10.2514/3.48818

[15] Whittingham B, Baker AA, Harman A, Bitton D. Micrographic studies on adhesively bonded scarf repairs to thick composite aircraft structure. Composites Part A: Applied Science and Manufacturing. 2009;**40**:1419-1432. DOI: 10.1016/j.compositesa.2008.12.011

[16] Baker A, Dutton S, Kelly D. Composites materials for aircraft structures. 2nd ed. American Institute of Aeronautics and Astronautics (AIAA) Publication Series; 2004. 601 p. DOI: 10.2514/4.861680

[17] Bekas DG, Tsirka K, Baltzis D, Paipetis AS. Self-healing materials: A review of advances in materials, evaluation, characterization and monitoring techniques. Composites Part B: Engineering. 2016;**87**:92-119. DOI: 10.1016/j.compositesb.2015.09.057

[18] Diesendruck CE, Sottos NR, Moore JS, White SR. Biomimetic self-healing. Angewandte Reviews. 2015;**127**:10572-10593. DOI: 10.1002/anie.201500484

[19] Williams G, Trask R, Bond I. A self-healing carbon fibre reinforced polymer for aerospace applications. Composites Part A: Applied Science and Manufacturing. 2007;**38**:1525-1532. DOI: 10.1016/j.compositesa.2007.01.013

[20] White SR, Moore JS, Sottos NR, Krull BP, Santa Cruz WA, Gergely RCR. Restoration of large damage volumes in polymers. Science. 2014;**344**:620-623. DOI: 10.1126/science.1251135

[21] Varley RJ, Craze DA, Mouritz AP, Wang CH. Thermoplastic healing in epoxy networks: Exploring performance and mechanism of alternative healing agents. Macromolecules Materials and Engineering. 2013;**298**:1232-1242. DOI: 10.1002/mame.201200394

[22] van Gemert GML, Peeters JW, Sontjens SHM, Janssen HM, Bosman AW. Self-healing supramolecular polymers in action. Macromolecules Chemistry and Physics. 2012;**213**: 234–242. DOI: 10.1002/macp.201100559

[23] Bai N, Saito K, Simon GP. Synthesis of a diamine cross-linker containing Diels-Alder adducts to produce self-healing thermosetting epoxy polymer from a widely used epoxy monomer. Polymer Chemistry. 2013;**4**:724-730. DOI: 10.1039/C2PY20611K

[24] Brunsveld L, Folmer BJB, Meijer EW, Sijbesma RP. Supramolecular polymers. Chemical Reviews. 2001;**101**:4071-4098. DOI: 10.1021/cr990125q

[25] Cordier P, Tournilhac F, Soulie-Ziakovic C, Leibler L. Self-healing and thermoreversible rubber from supramolecular assembly. Nature. 2008;**451**:977-980. DOI: 10.1038/nature06669

[26] Palmer LC, Velichko YS, de la Cruz MO, Stupp SI. Supramolecular self-assembly codes for functional structures. Philosophical Transactions of the Royal Society A. 2007;**365**: 1417-1433. DOI: 10.1098/rsta.2007.2024

[27] Brunsvel L, Folmer BJ, Meijer EW, Siblesma RP. Supramolecular polymers. Chemical Reviews. 2001;**101**:4071-4098. DOI: 10.1021/cr990125q

[28] Greenland BW, Hayes W, Colquhoun HM. Design, synthesis and computational modeling of aromatic tweezer-molecules as models for chain-folding polymer blends. Tetrahedron. 2008;**64**:8346-8354. DOI: 10.1016/j.tet.2008.05.077

[29] Iyer PK, Beck JB, Rowan SJ. Synthesis and optical properties of metallo-supramolecular polymers. Chemical Community. 2005;**41**:319-321. DOI: 10.1039/B410734A

[30] Kalista SJ, Ward TC. Thermal characteristics of the self-healing response in poly (ethylene-co-methacrylic acid) copolymers. Journal of Royal Society Interface. 2007;**4**:405-411. DOI: 10.1098/rsif.2006.0169

[31] Sijbesma RP, Beijer FH, Brunsveld L, Folmer BJB, Hirschberg JHKK, Lange RFM, Lowe JKL, Meijer EW. Reversible polymers formed from self-complementary monomers using quadruple hydrogen bonding. Science. 1997;**278**:1601-1604. DOI: 10.1126/science.278.5343.1601

[32] Söntjens SHM, Renken RAE, van Gemert GML, Engels TAP, Bosman AW, Janssen HM, Govaert LE, Baaijens FPT. Thermoplastic elastomers based on strong and well-defined hydrogen-bonding interactions. Macromolecules 2008;**41**:5703-5708. DOI:10.1021/ma800744c.

[33] Kostopoulos V, Kotrotsos A, Tsantzalis S, Tsokanas P, Loutas T, Bosman AW. Toughening and healing of continuous fibre reinforced composites by supramolecular polymers. Composites Science and Technology. 2016;**128**:84-93. DOI: 10.1016/j.compscitech.2016.03.021

[34] Kostopoulos V, Kotrotsos A, Baltopoulos A, Tsantzalis S, Tsokanas P, Loutas T, Bosman AW. Mode II fracture toughening and healing of composites using supramolecular polymer interlayers. eXPRESS Polymer Letters. 2016;**10**:914-926. DOI: 10.3144/expresspolymlett.2016.85